SCARBOn
SPACE CARBON OBSERVATORY next step

SCARBOn Project: NanoCarb Prototype Test Report (public version)

Document produced by	**J. Rodrigo & B. Laulan—Souilhac (Absolut System)** **S. Gousset (University of Grenoble)**

Release date	**30/07/2026**
Project name	**SCARBO next step - Space CARBon Observatory' solution to improve monitoring of GHG emissions and help establishing reliable data for emission trends forecasts (SCARBOn)**
Project number	**101135301**
Project starting date	**01/01/2024**
Project duration	**40 months**
Project coordinator	**Airbus Defence and Space SAS**
Project website	**https://www.scarbon-project.eu/**

Co-funded by the European Union

Co-funded by the European Union. Views and opinions expressed are however those of the author(s) only and do not necessarily reflect those of the European Union or the European Health and Digital Executive Agency (HADEA). Neither the European Union nor the granting authority can be held responsible for them.

Export Control Information concerning this document's content

1. **European regulation controlled content**
Country of origin for controlled data in this document: ☐ BELGIUM ☐ CZECHIA ☒ FRANCE ☐ GERMANY ☐ NETHERLANDS ☐ SPAIN

☒ Does not contain national dual-use or war material controlled data. ☐ These commodities, technology or software are controlled by the European Union in accordance with dual-use regulation 428/2009 under classification [XXXX]. ***(See applicable export license information in Dispatch Note)***

2. **US Regulation controlled content**
☒ Does not contain US origin EAR or ITAR controlled data. ☐ These commodities, technology or software are exported in accordance with the United States Export Administration Regulations. Diversion contrary to U.S. law is prohibited. These commodities, technology or software are controlled under ECCN [YYYY]. (See applicable export license information in Dispatch Note)

Export Control Information questionnaire filled out by: J. Rodrigo

SCARBOn participants

Participant No	Legal name	Short name	Country
1	Airbus Defence and Space SAS (COORDINATOR)	Airbus-F	FR
1.1	Airbus DS Geo SGSA (affiliated entity)	Airbus-ES	ES
2	Airbus Netherlands B.V.	Airbus-NL	NL
3	Absolut System SAS	Absolut	FR
4	Université Grenoble Alpes	UGA	FR
5	Centre National de la Recherche Scientifique	CNRS	FR
6	GRANT Garant s.r.o.	GG	CZ
7	Institut Royal d´Aéronomie Spatiale de Belgique	BIRA-IASB	BE
8	Office National d'Etudes et de Recherches Aérospatiales	ONERA	FR
9	Deutsches Zentrum für Luft- und Raumfahrt e.V.	DLR	DE
10	Institut Cartogràfic i Geològic de Catalunya	ICGC	ES

Table of contents

List of abbreviations

Abbreviation	Definition
CH4	Methane
CO2	Carbon Dioxide
FP	Fabry-Perot
FPA	Focal Plane Array
FTIRS	Fourier Transform Infra-Red Spectrometer
FWHM	Full Width at Half Maximum
IPAG	Institut de Planétologie et d´Astrophysique de Grenoble
ISRF	Instrumental Spectral Response Function
InGaAs	Indium, Gallium, Arsenic infra-red detector
ISRF	Instrumental Spectral Response Function
IR	Infrared
MOCVD	Metalorganic Chemical Vapour Deposition
MTF	Modulation Transfer Function
NanoCarb	Name of existing interferometer instrument
NanoCarb-P	NanoCarb design for airborne prototype
L0	Level 0 data, corresponding to a raw NanoCarb acquisition

Abbreviation	Definition
L1	Level 1 data, corresponding to co-registered datacube or interferograms
L2	Level 2 data, corresponding to the retrieve gas concentration
LTM	Laboratoire des Technologies de la Micro-électronique (Micro-electronics Technology Laboratory)
OCT	Optical Coherence Tomography
ONERA	Office national d'études et de recherches aérospatiales (National Office for Aerospace Studies and Research)
PECVD	Plasma-Enhanced Chemical Vapor Deposition
UGA	Université Grenoble Alpes (Alps Grenoble University)
PSF	Point Spread Function
PVD	Physical Vapor Deposition
UV	Ultra-Violet
WP	Work Package

List of reference/applicable documents

Document title	Document author	Date of issuance
SCARBOn D4.1 NanoCarb-P Design Report	ONERA	October 2024 (project report)

List of Tables

List of Figures

1 Executive Summary

1.1 SCARBOn Overview

SCARBOn (Space CARbon Observatory Next step) is an innovation action project funded under the Horizon Europe Programme. It is the continuation of the Horizon 2020 SCARBO project. SCARBOn is a multidisciplinary project carried out by a gender-diverse team, through a consortium including the space industry, SMEs and scientific institutes. It is led from Toulouse, France by Airbus Defence and Space. SCARBOn project started in January 2024, with a total 40 months of implementation.

The main objective for the of the SCARBOn collaborative project is to mature the SCARBOn overall system based on a constellation of small satellites - with miniaturised static spectrometer concept (NanoCarb) coupled with aerosol sensors (SPEXone) - that will be able to monitor greenhouse gases (GHG) – notably the CO_2, and CH_4 as well – from space. The instruments together will deliver daily accurate global measurements to monitor the diurnal variations of fossil CO_2 emission. This CO_2 and CH_4 anthropogenic emissions monitoring data aims to be a valuable contributor to the European Commission's endeavour to fight climate change. As an upside, the monitoring data will foster the development of added-value services and will represent a state-of-the-art European alternative to the burgeoning non-European commercial initiatives.

The SCARBOn project maturation is articulated over the detailed technical definition of the NanoCarb instrument, the industrial definition of both instruments and the constellation concept confirmation, targeting an operational system availability before the end of the decade. The design of the NanoCarb instrument will be upgraded and refined following the outcomes of the previous SCARBO study, and its performances will be carefully modelled. An instrument breadboard will provide valuable data during an airborne campaign, which will be used together with modelled data to verify the instrument design. This will allow raising the instrument TRL to at least 5 by the end of the project. Furthermore, data processing at levels L1 to L4 will validate the concept capability to monitor GHG plumes from space.

1.2 Document summary

This document is the public version of the SCARBOn project deliverable D4.2 NanoCarb-P Test Report. It is published for informational purposes only and has not been approved by European Health and Digital Executive Agency (HADEA), the granting authority.

This document presents a comprehensive overview of the optical characterization, optical test and thermal test campaigns, as well as the associated performance improvements, conducted by Absolut System and UGA-IPAG on NanoCarb-P prototype.

It presents tests performed on the NanoCarb-P cameras, covering three levels of integration: at the end of the three steps of integration.

- The first part is dedicated to the **optical components characterization**. These measurements aim to follow the development of the optical elements and to validate their compliance with the optical performances.
- The second part is dedicated to the **NanoCarb-P optical tests** carried out at the integrated instrument level. These tests aim to verify the correct integration and alignment of the optical components with the detector, as well as to validate optical assembly performance.

The third part is dedicated to the **thermal tests** on the complete camera. These tests are conducted to confirm the thermal behaviour of the NanoCarb-P CO2 and CH4 cameras under representative conditions and to consolidate the results in preparation for the airborne measurement campaign.

2 Optical components characterization & validation

This section describes the optical characterizations, mainly lead by UGA-IPAG, with support from ONERA, and gathers some of the tests performed by the subcontractors. The tests have been achieved at component level before integration in order to support technological investigation and to validate the delivered component regarding specifications.

2.1 Introduction

Investigations presented here concern the components inside the NanoCarb interferometric core, upgraded within SCARBOn WP4:

1) The silicon interferometric plate,

2) Coating of the interferometric plates,

3) The Narrow-band-filter.

Components are tested independently to control their characteristics regarding specifications, then to select the best among those manufactured to be implemented in the prototypes.

2.2 Interferometric plate

2.2.1 Manufacturing process recall

The Figure 1 recalls the manufacturing process of the silicon interferometric plates, starting from 100 mm-wafer to 20 x 20 mm² NanoCarb-P chips, using grayscale lithography and plasma etching. Some pictures of the exposed resist, then of the pattern transferred into the silicon are presented on Figure 1.

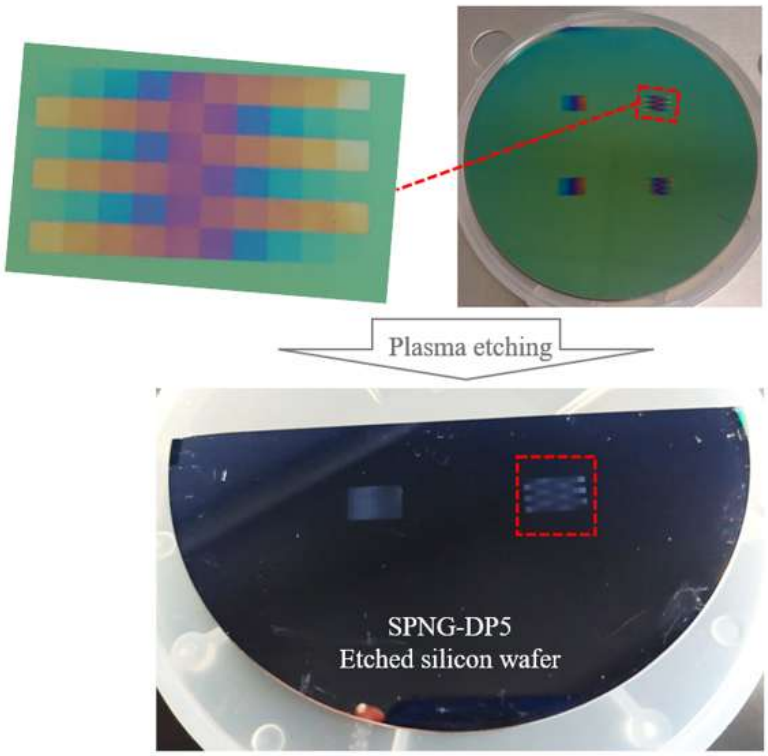

Figure 1: Top: photo-colorimetric control of the exposed resist; Bottom: transferred pattern over the silicon wafer [Credit UGA-LTM]

Main thicknesses of the interferometers have been specified in D4.1. To reach the CO2 plate target specification, the wafers were ordered directly at the correct thickness, with some other specifications about purity and face parallelism. For the CH4 plate, target thickness has been obtained by thinning the same batch of wafer, using grinding technic.

The number of etched interferometers per chip, the difference in depth between two interferometers, and the total etched depth, result from trade-offs between D4.1 specifications and capabilities of the used platforms.

Many efforts have been provided by UGA-LTM to select the optimal resist with the best characteristics, then to optimize exposure parameters to manage the transfer of the geometrical pattern defining the interferometer array into the silicon. Main concerns are the spatial flatness of each etched interferometer, and roughness of the etched surfaces, resulting from this transfer and exposure homogeneity.

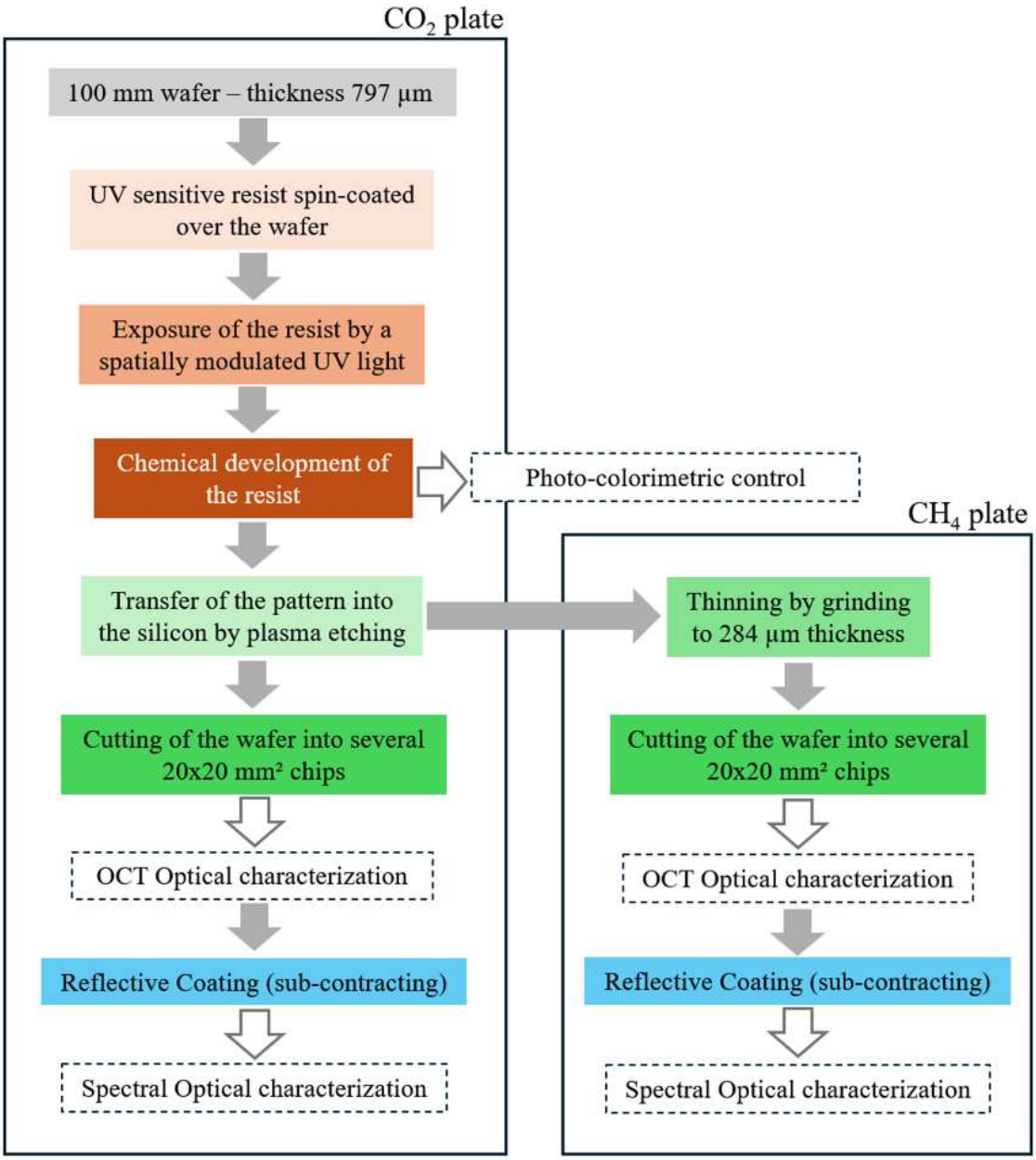

Figure 2: Manufacturing and test pipeline for the interferometric plates

2.2.2 Characterization methodology and objectives

We focus here on the optical characterization of the final delivered 20x20 mm² chips before coating, coming from two wafers: SCARBN-7 for CO2 and SCARBN-9 for CH4. Many other batches have been processed by UGA-LTM then characterized by UGA-IPAG before to optimize manufacturing process, but they will be not presented here.

The main parameters to be validated are the optical roughness in transmission of the etched interferometers, planarity of each interferometer, total etched thickness and profile. To achieve this, an imaging Optical Coherence Tomography technic have been implemented in the first SCARBO project, using a Michelson interferometer. The method is described in [Ehrhardt 2018] and allows to quickly be obtained map of relative optical thickness in transmission of the interferometric plate without spatial scanning of the sample.

2.2.3 Experimental setup

The used optical bench is presented on Figure 11. It implies an incoherent light source at 1600 nm of wavelength, with a spectral bandwidth of 50 µm. The delay line allows to introduce nanometric displacements is z-axis, producing controlled interferences over the detector. The detector is a SNAKE InGaAs detector, similar to the ones integrated in the NanoCarb prototypes: 640 x 512 pixels of 15 µm, with a thermal regulation. The sample is directly placed in front of the detector, in collimated beam. This configuration allows to map intensity modulations relied on optical thickness of the sample, simply by controlling the delay line position. The whole sample is captured over the area of the detector, without need to scan in x and y axis.

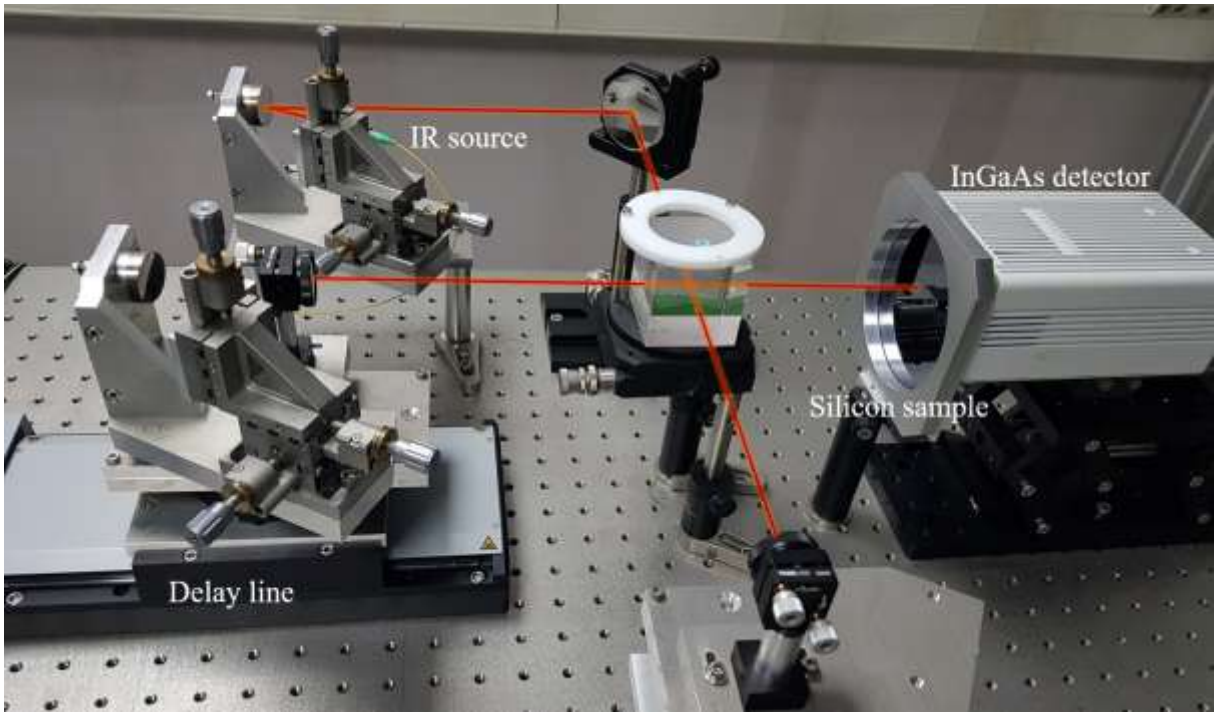

Figure 3: UGA-IPAG imaging Optical Coherence Tomography bench used for interferometric palte characterization

The map of relative optical thickness is obtained by correlating wave packet from each pixel regarding a reference over the sample. This technic gives a very good relative accuracy (better than 1 mechanical nm), but a poor absolute accuracy (~1-10 µm). Hence, it implies to unwrap phase map with complex pattern due to the geometry of the interferometer array, leading to inexact profiles of thickness at large scale, with biased steps and artefacts. The presented tests could be complemented in that way by additional characterizations, using e.g. classical FTIRS with integrated optical rule.

2.2.4 Results

Map of relative optical thickness obtained for the CO2 chip SCARBN7-A and for the CH4 chip SCARBN9-C, both integrated then in the NanoCarb-P cameras, are presented on the Figure 5. A standard deviation is computed for each sub-aperture (and plotted in blue), to provide an estimate of the roughness and of the impact of the topology over the optical quality.

i) Those maps make clearly appearing the pattern of 10 x 6 etched square interferometers over the silicon. This number of interferometers was expected as it corresponds to the maximum area that can be etched onto the platform used (PTA). We can observe, in the configuration used in this experiment, that the size of the map matches perfectly the size of the detector used in the NanoCarb prototype. So, the size of one sub-aperture in these maps is strictly the same than for NanoCarb-P (64 x 64 pixels, and 960 x 960 µm²).

Given that we expect 10 x 8 sub-apertures (or thumbnail) in the NanoCarb-P, and that only 10 x 6 interferometers are etched here, a non-eched surface of the plate, corresponding to 10 x 2 interferometers, will be used in the NanoCarb build. This non-etched surface, optically active, is also characterized on the Figure 5 (on the bottom of the top map e.g.).

ii) Some abrupt transitions are visible on these maps, especially at the interface between some row of interferometers. These artefacts are purely numerical, induced by a bad phase unwrapping when the step is higher than one wavelength. Nevertheless, some defects in the silicon are visible, especially on the top-left corner of the CO2 plate, and close to the middle-left of the CH4 plate. It has been identified that these defects are induced by a gas release from the resist during the plasma etching, or by contaminants. The corresponding standard deviation for these thumbnails is clearly drastically increased (~50 nm mecha.), which impacts the optical quality, both in terms of image formation and interferometric contrast. Since this involves only one defective channel out of 80 thumbnails, the impact on the final performance is very minor and acceptable. This defect over the CO2 plate can be observed by naked eyes as visible on the Figure 4.

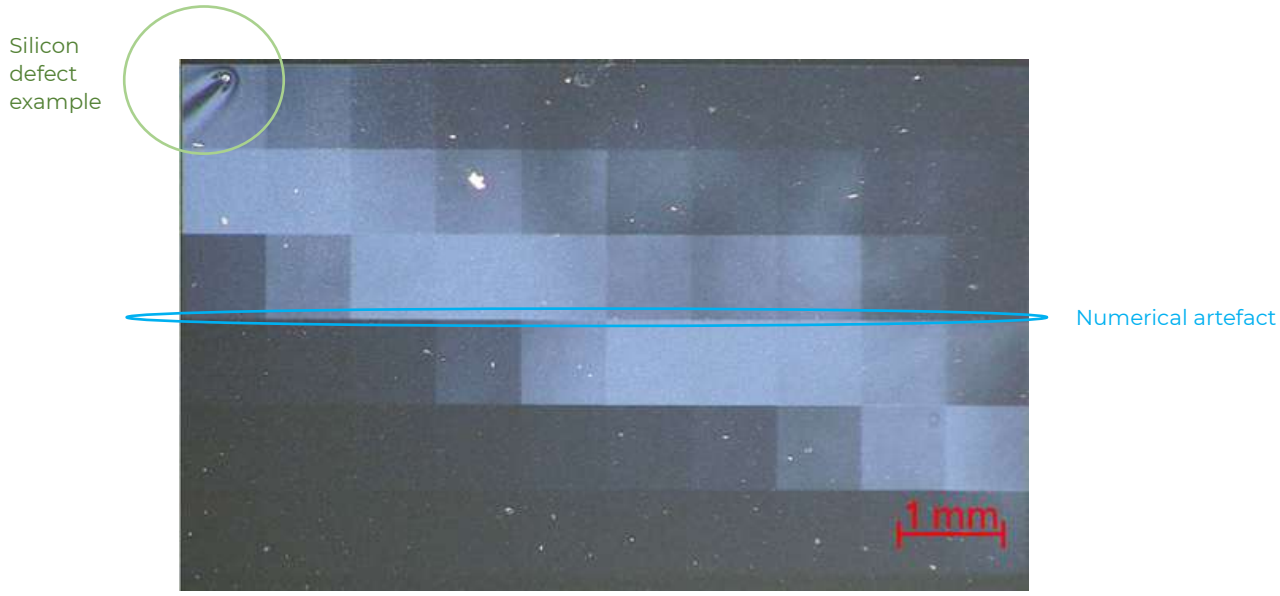

Figure 4: Microscopic view of the CO2 SCARBN-7-A chip

iii) Excepted the one or two impacted thumbnails, the standard deviation over the etched area is generally ranged between 5 and 10 nm mecha., while it is below 5 nm over the non-etched area, showing a small effect of the etching over the roughness. The values are slightly superior for the CH4 plate, showing probably an impact of the grinding step, both over the roughness and over surface topology.

Some horizontal profiles are drawn on Figure 6 for each row of etched interferometers, but also over the non-etched area (dashed blue line):

iv) We clearly observe a topology over the chips, even over the non-etched area: a slope of 100 nm mecha. from left to right for the CO2 plate, and a rounded shape of 200 nm peak to

valley for the CH4 plate. In the case of the CO2 plate, this topology was probably already present on the wafer prior to the processing, as silicon suppliers do not guarantee thickness variations bellow a few micrometres. For the CH4 plate, the shape suggests a distortion caused by the thinning process, or a deformation after due to the small thickness of the plate. Anyway, at the scale of a sub-aperture, the variations are below 10 nm and seems to be the main contributor to the standard deviation per thumbnail. This order of magnitude has a neglectable impact over the performances.

v) Jumps between interferometers are visible over the profiles and are generally ranged between 20 and 30 nm mecha., as expected, but with some important variations. The regularity of the depth of etching is not crucial for the NanoCarb-P performances.

vi) The total depth of etching is not easy to evaluate from these maps, due to jump artefacts induced by phase unwrapping. We estimate for CO2 and CH4 a total depth of etching close to 400 nm mecha., with a target value higher than 300 nm.

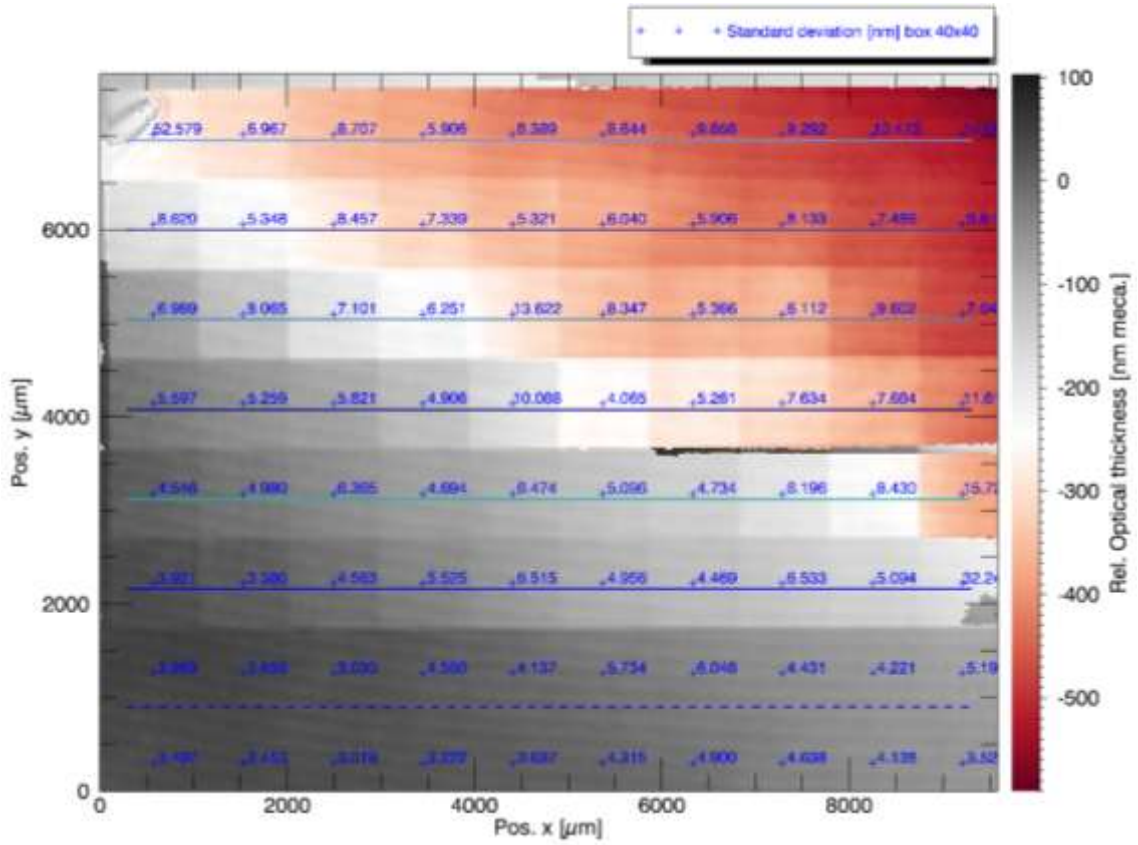

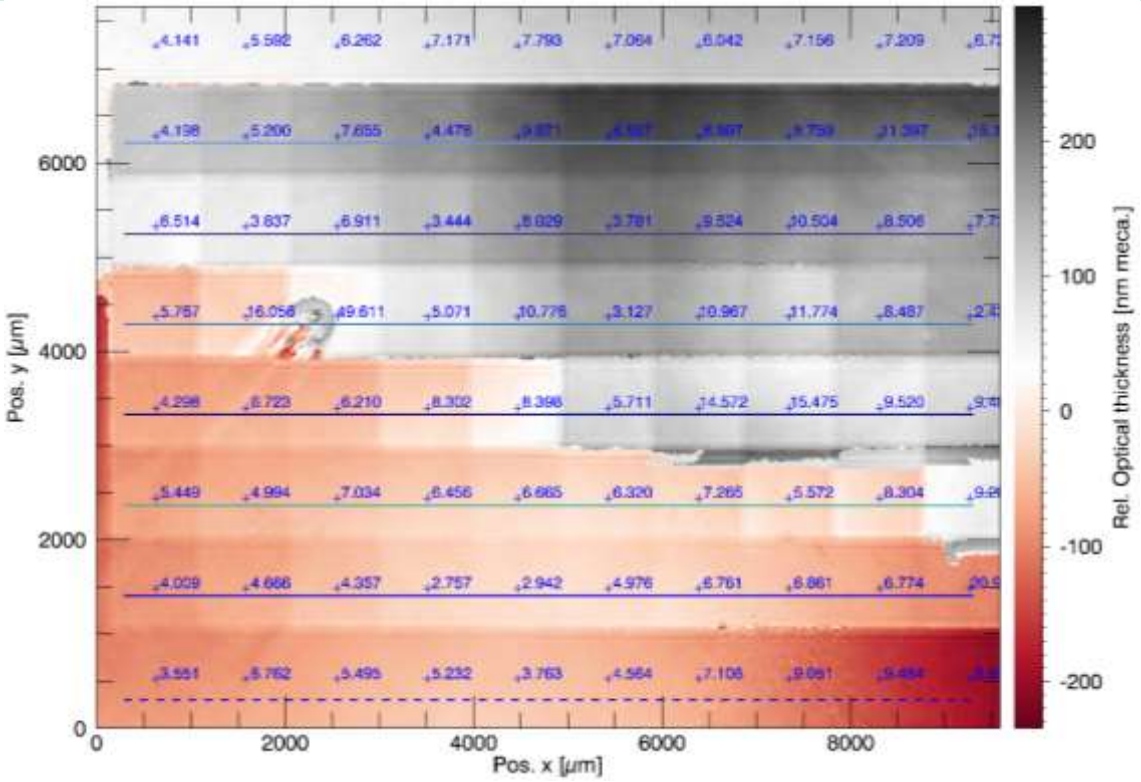

Figure 5: Characterization of the interferometric plates, before coating: relative optical thickness map, with standard deviation per sub-aperture in blue. Top: SCARBN-7-A CO2 plate; Bottom: SCARBN-9-C CH4 plate

Profiles over the coloured lines are plotted below:

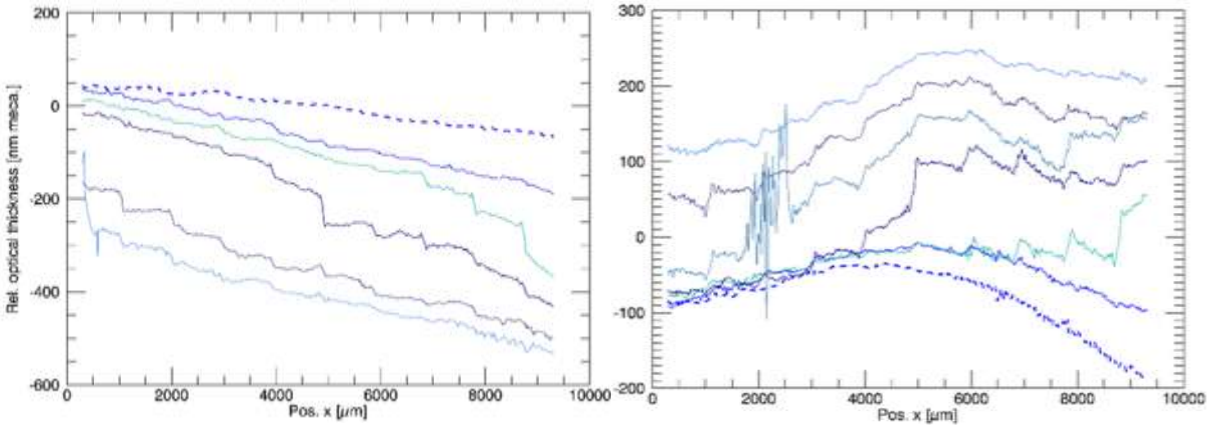

Figure 6: Horizontal profiles over the interferometric plates. Left: SCARBN-7-A CO2 plate; Right: SCARBN-9-C CH4 plate. Each coloured line refers to the same line over the relative optical thickness map. The dashed line is on a non-etched area of the plate

These measured characteristics are summarized on the following table. Measured dispersion of the single step depth is not critical, as it does not impact the performance: the total depth of etching is more crucial regarding the final sensitivity, as well as a quiet homogeneous distribution of thickness over the range.

Parameters	Specification	CO2 plate (SCARBN-7-A)	CH4 plate (SCARBN-9-C)
Number of etched interferometers	10 x 6	10 x 6	10 x 6
Standard deviation per thumbnail	σ < 20 nm meca. rms (*)	5 - 9 nm (processed area) 5 – 14 nm (processed area)	5 – 14 nm (processed area) 4 – 9 nm (native area)
Total depth of etching	> 300 nm mecha.	~ 400 nm	~400 nm
Single step depth	20 nm	20 – 30 nm	20 – 30 nm
Inoperant thumbnails	Threshold: σ > 15 nm (**)	1	2

Table 1: CO2 and CH4 interferometric plates characterization results before coating

(*) Criterion from [HARIHARAN, Parameswaran. Optical interferometry, 2e. Elsevier, 2003, Losses in Fabry–Perot interferometers], based of loss of reflectivity in Fabry-Perot by surface scattering effect:

$$\frac{\sigma}{\lambda} \ll \frac{\sqrt{1-R}}{4\pi}$$

With σ the roughness in nm mecha., and R the surface reflectivity. In our case, we compute a standard deviation per sub-aperture, mainly dominated by topology, which is a better situation, with a lower impact over reflectivity.

(**) This criterion allows to discriminate the thumbnails impacted by strong defects in the silicon.

2.3 Interferometric plate reflective coating

2.3.1 Framework

The coating is the last step of the interferometric plate manufacturing process presented on Figure 2. It allows to increase surface reflectivity of the interferometers, and thus to improve the selectivity of the spectral modulation for CO2 or CH4 regarding other atmospheric parameters like water vapor, albedo, … It has thus been shown in D4.1 than an optimal surface reflectivity of 55% for CO2 and 78% for CH4 (compared to ~33% for native silicon) could lead to improve the sensitivity up to a factor two regarding the old SCARBO design, and to decrease correlation between albedo and gas absorption in the signal.

At the beginning of WP4, single layer metallic coating has been intensively investigated, as it offered simple and cost-effective opportunities to use a research platform in UGA. Until July 2025, many combinations of material and technics have been tested and characterized at UGA: Gold, Gold + Chromium, Silver, Gold+Titanium, coating of one single face, of the two faces, with both Physical Vapor Deposition (PVD), then E-Beam Metal Evaporation over the PTA platform in Grenoble. All have shown poor results: poor repeatability and high absorption regarding obtained reflectivity.

Another kind of coating have been thus decided for the airborne prototypes, using multi-layer dielectric material. This step has been sub-contracted by *Institute Fresnel* in France.

We show below the results obtained for the two kinds of coating.

2.3.2 Objective and methodology of the test

Checked parameters within SCARBOn are surface reflectivity and peak transmission over the relevant CO2 and CH4 spectral bandwidths. These parameters are mapped across the entire optical surface of the samples, in order to check spatial homogeneity of the coating.

We derive these parameters from spectral transmission maps, obtained by a monochromatic spectral scan within collimated beam of the samples. Data are processed using an inverse model of a Fabry-Perot interferometer (T_{peak} as a function of $R_{surface}$). The results are finally compared to thin film numerical simulations using refractive index from the literatures for the metallic coating.

2.3.3 Experimental setup

A tuneable laser source is collimated then placed in front of an InGaAs detector. A monochromatic scan is performed in this configuration, then redo after placing the sample in between the camera and the source. Dividing the two scan allows to obtain a transmission map of the sample, assuming a good stability and repeatability of the scan. A wavemeter is used in parallel to synchronously monitor the exact wavelength of the source.

A dedicated collimator has been used, but also the bench of Figure 3 with the delay line hidden and the incoherent light replaced by the tuneable laser.

2.3.4 Results

- **Single layer metallic coating by Gold**

Many coating configurations have been extensively stressed during the first reference period of SCARBOn. We present here only the final coating test realized by UGA-LTM with the CO_2 chip batch SCARBN-7, intended to be integrated into the NanoCarb-P cameras.

Model fitting example of the data measured is presented on Figure 7. The model converges to a surface reflectivity of 54%, very close to the specifications, but also to a peak transmission only of 22%.

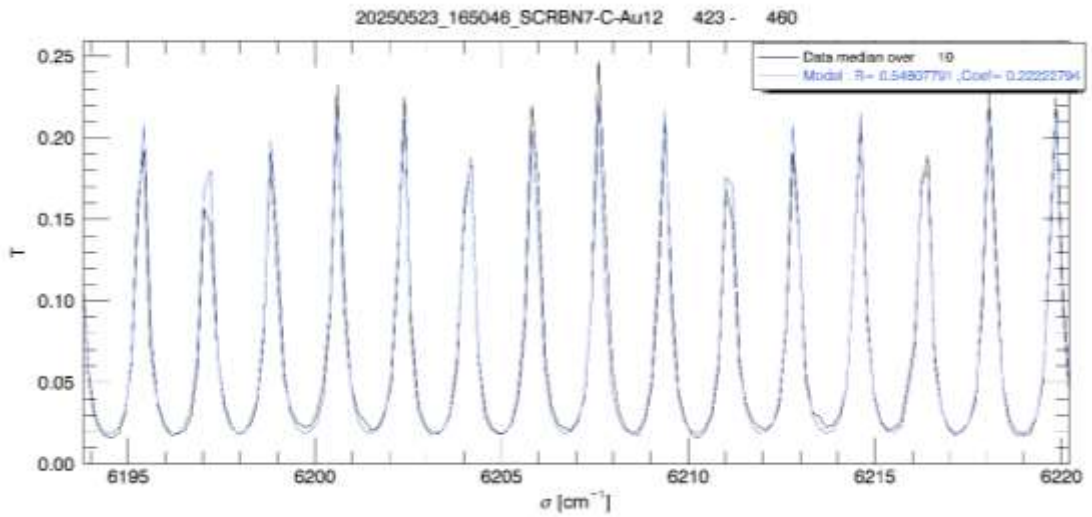

Figure 7: SCARBN-7-C CO2 chip + 12 nm of gold over the two faces. Model fitting example over one single pixel (median over an area of 10 x 10 pixels)

A thin film simulation is presented on Figure 8, for a thickness of gold of 8 nm on the two faces. This thickness allows to reproduce the surface reflectivity around 55%. But in the case of this simulation, the expected peak transmission is higher than 60%, three times higher than the transmission obtained in the test batch.

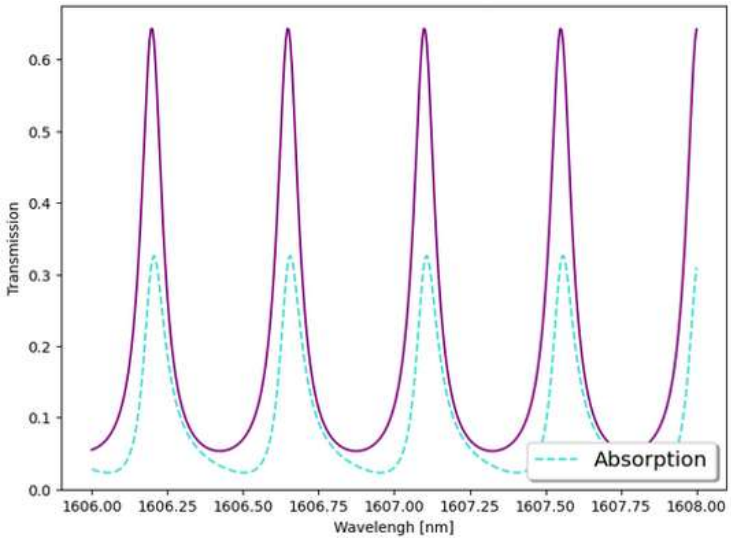

Figure 8: Thin film simulation of a gold-coating of 8 nm over a 797 µm silicon substrate (Refractive index from [Olmon 2012 Evaporated gold]). Purple curve shows the transmission pattern, and dotted line the absorption in the material.

Several considerations lead us to abandon the single layer metallic coating in favour of a multi-layer coating:

- The obtained coatings were too absorbent, leading to a loss of signal to noise ratio. Nevertheless, a peak transmission between 30% and 60% could have been offset by increasing the exposure time of the acquisitions during the flights. With 25% of transmission in the best case, this coating would not have permit to improve the performances even with the target surface reflectivity reached.
- The used platform does not have in situ control of the layer thickness. Hence, its repeatability was too low, avoiding applying a relevant offset correction from one batch to another.
- It was difficult to specify the thickness of the layer, because the simulations are extremely dependant of the reference used in the literature for the refractive index of the coating material. Obtaining a complete characterization of the refractive index for the coating material would be interesting to improve the performances.

After this test, SCARBN-7 batch has been washed (with ultra-sonic bath and acetone) to be re-coated with a multi-layer dielectric coating.

- **Multi-layer dielectric coating:**

The sub-contractor (*Institute Fresnel, UMR7249 France*) provided the characterization presented on Figure 9, showing a good adequacy between theory (specifications) and measures at global scale.

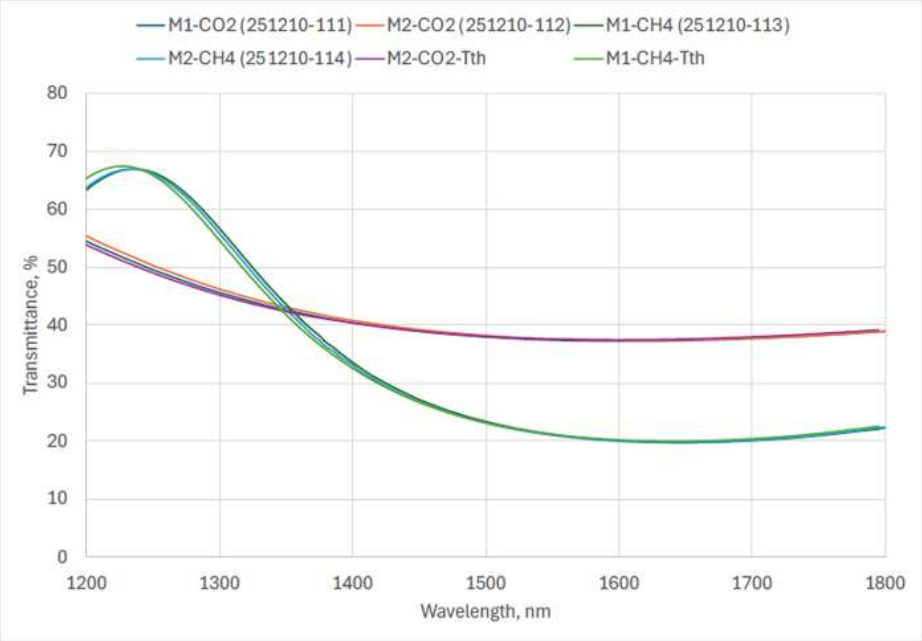

Figure 9: Multi-layer dielectric coating characterization over the sample made by Institute Fresnel [Credit: Fresnel Institute UMR7249]. The measures are made with only one single coated face

Figure 10 and Figure 11 show the characterization maps obtained at UGA-IPAG with the multi-layer dielectric coating. These characterizations concern the CO2 chip SCARBN-7-A and the CH4 chip SCARBN9-C, integrated in January 2026 in the NanoCarb-P cameras for the SCARBOn airborne campaign.

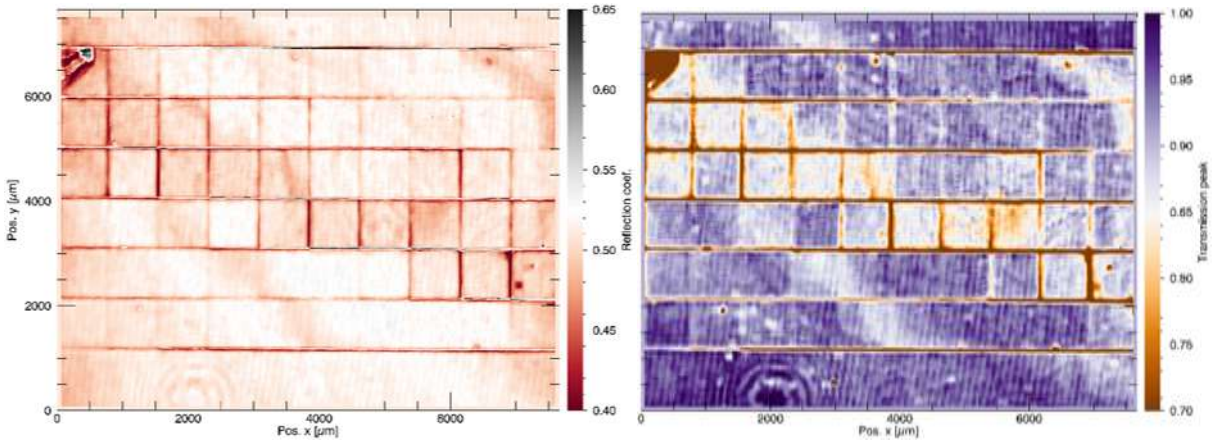

Figure 10: CO2 multi-layer dielectric coating characterization maps obtained at UGA-IPAG. Left: surface reflectivity map; Right: peak transmission map

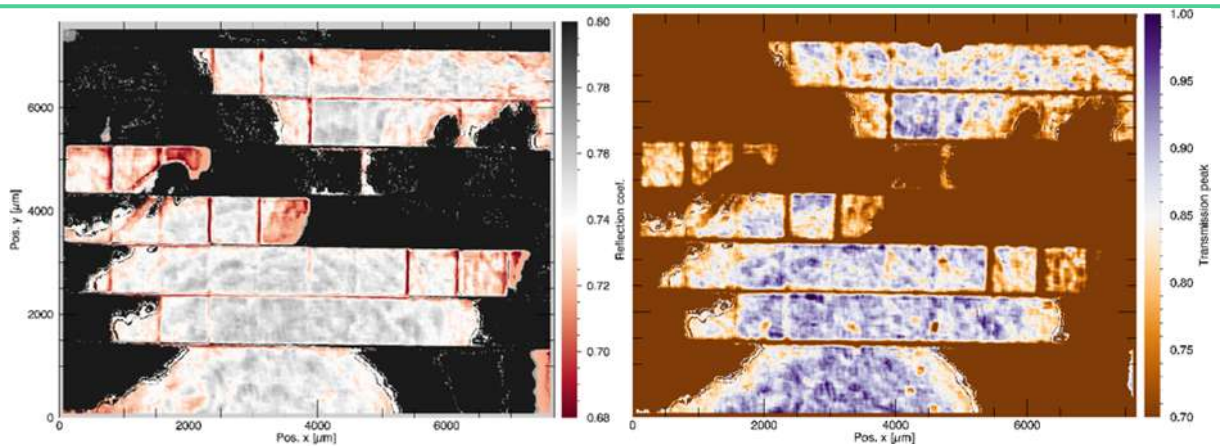

Figure 11: CH4 multi-layer dielectric coating characterization maps obtained at UGA-IPAG. Left: surface reflectivity map; Right: peak transmission map

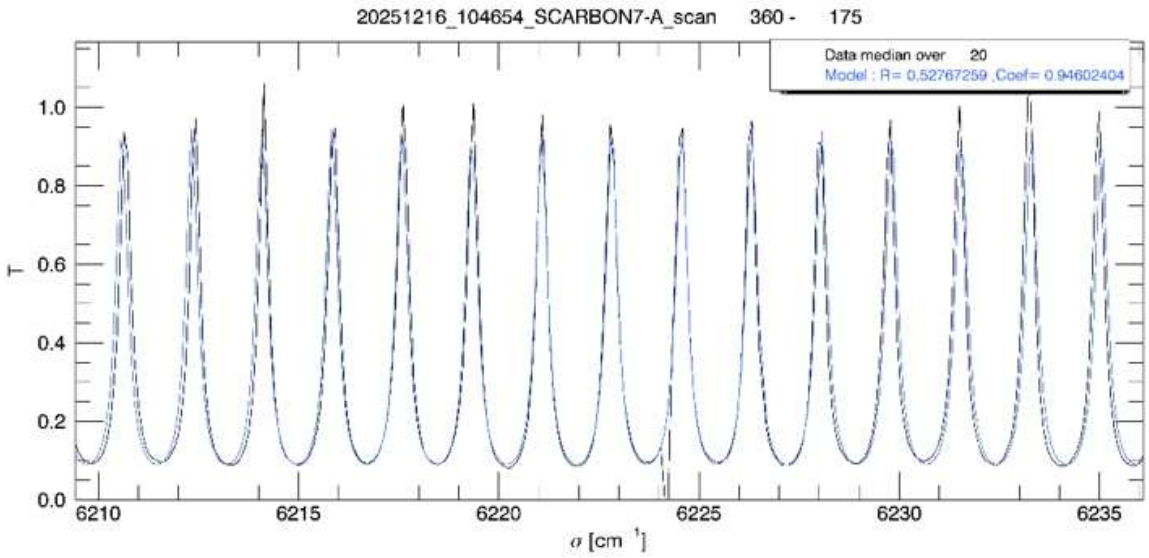

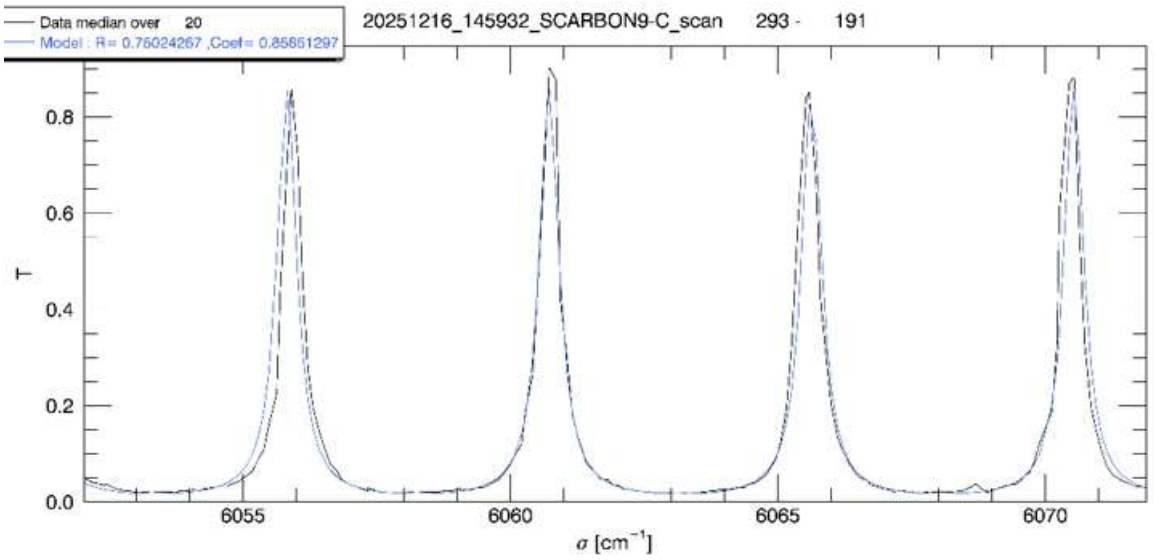

Figure 12: Multi-layer dielectric coating, model fitting example over one single pixel. Top: CO2 plate; Bottom: CH4 plate

The surface reflectivity and peak transmission maps presented Figure 10 and Figure 11 are obtained by fitting a Fabry-Perot analytical transmission model to the measured spectral transmission. Fitting examples of the data are presented on Figure 12. The measure is centred around the etched area of the interferometric plates. The interfaces between the Fabry-Perot present a degraded reflectivity and transmission, which can be induced by both measurement artefacts (diffraction at the edges), or by an inhomogeneous coating. In any way, these areas are masked by a pupil diaphragm in NanoCarb and have no impact over the performances.

We can also notice some interferometers with important inhomogeneities, as on the top-left side of the CO2 plate. This defect is not coming from the coating, as it can be observed on the characterization made on native silicon in 2.2.2. More generally, homogeneity of the coating seems to be ruled by roughness of the uncoated plates and by surface topology.

For the CH4 plate Figure 11, we observe some large areas where the fitting algorithm did not converge. In this case, the algorithm was very sensitive to guess parameters, and it has been very difficult to obtain a full fitting map with only a single run.

In the majority of cases, homogeneity of the coating does not vary more than a few percent at the scale of a single interferometer, and thus it is expected to have a negligible impact over the performances. The averaged value of surface reflectivity and peak transmission are presented on Table 2 and reach the specifications.

Plate	Transmission peak		Surface reflectivity	
	Spec.	Obtained	Spec.	Obtained
CO2 plate SCARBN-7-A)	> 80 %	94 (average)	55% +/-5	51.5 (average)
CH4 plate (SCARBN-9-C)	> 50 %	85 (average)	78% +/-4	74.5 (average)

Table 2: Multi-layer dielectric coating characterization results

2.4 Narrowband filter

This section has been omitted from the public version of the report as it contains sensitive information. The complete report is available to the relevant project stakeholders.

3 NanoCarb-P optical testing

3.1 Introduction

This section describes the optical test performed at system level, after integration of the optical component into NanoCarb-P cameras. The test aims to validate the whole system and its performances, and to provide calibration data used in the data processing pipeline of the airborne campaign.

3.2 NanoCarb-P Integration

The new coated CO2 and CH4 interferometric plates have been integrated into the dedicated NanoCarb-P demonstration cameras, to replace the old plates manufactured during SCARBO. We replaced also the CH4 narrow-band filter with the new high index filter developed during SCARBOn, while we kept the previous CO2 filter in place. We conserved also in place the microlenslet arrays. The 3D layout of NanoCarb demonstration camera is presented on Figure 13. A dedicated Peltier module allows to thermally regulate the interferometric core (b+c+d+e+f on the following figure) + front objective (a). Another independent Peltier module regulates the detector (g).

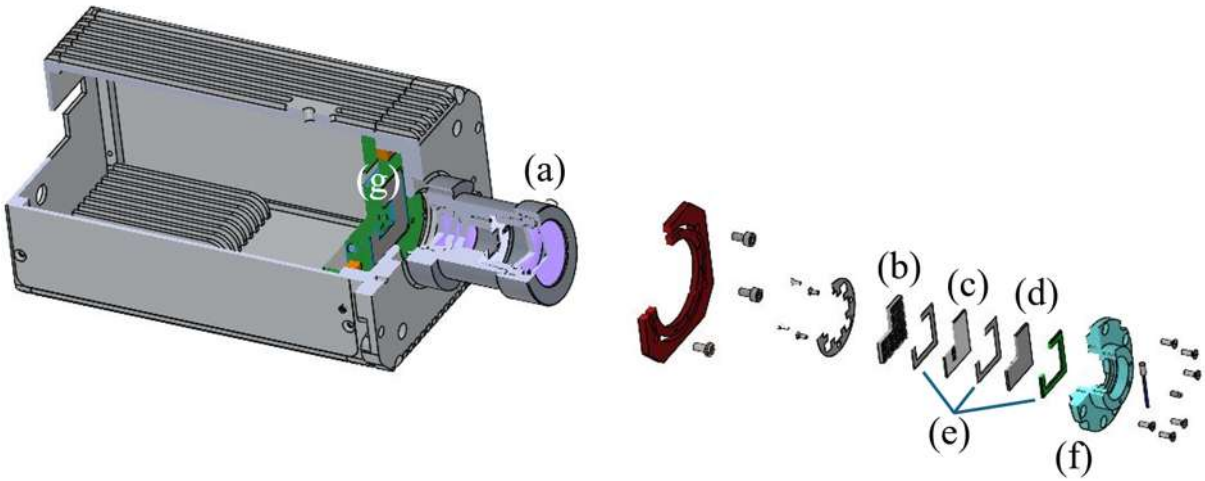

Figure 13 NanoCarb demonstration camera 3D view. (a) front objective; (b) 10x8 microlenslet array; (c) interferometric silicon plate; (d) Narrow-band filter; (e) spacers; (f) Mechanical housing of the interferometric core; (g) Detector; (f) is integrated between (g) and (a), inside the camera mechanical housing

Integration of the new components started the 19th of January 2026, involving a team from UGA-IPAG, Absolut System, and ONERA, in the UGA-IPAG laboratory. Some pictures during the integration are presented on Figure 14, Figure 16 and Figure 16.

Figure 14: Integration of NanoCarb-P CO2 camera: mounting the interferometric core and Left: coated CO2 interferometric plate.

Figure 15: Integration of NanoCarb-P CO2 camera: left: alignment of the interferometric core regarding the detector and right: experimental setup for the alignment

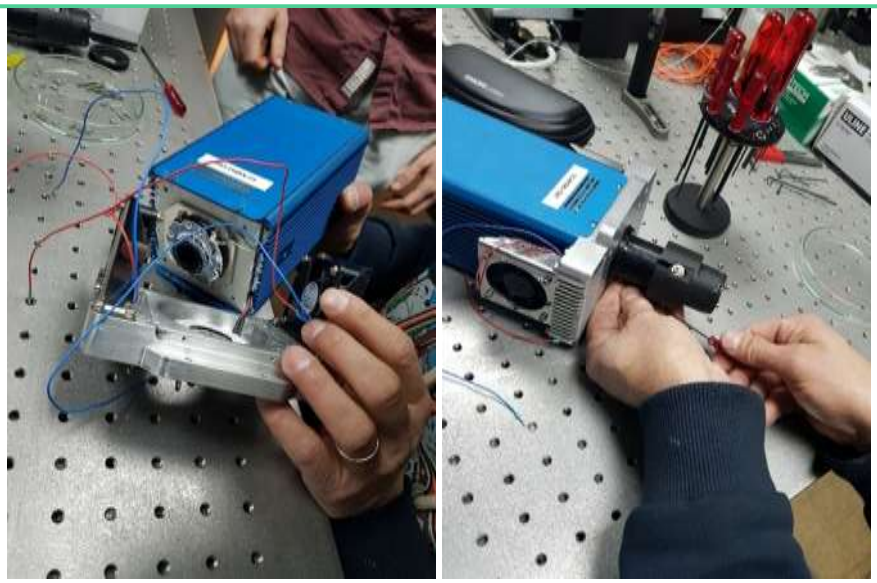

Figure 16: Left: installing the front face + Peltier module in contact of the interferometric core and right: the NanoCarb-P CO2 camera with front face and objective mounted

3.3 Spatial characterization

3.3.1 Objectives and methodology

We investigate here the imaging performances of the NanoCarb-P CO2 et CH4 cameras:

- **Optical quality**: validation test to ensure a correct alignment of the optics.
- **Mapping of inter-thumbnails distortions**: very important to provide calibration data, used to process the acquisitions from the airborne campaign (thumbnails co-registration).
- **Ghost images**: investigation to support space instrument design.

These analyses are based on acquisitions performed at UGA-IPAG, using a collimated source and a goniometer. Its purpose is to scan the field of view of the cameras with a point image. The experimental setup is shown on Figure 17. We move the point image in a grid of 33 x 33 positions in the field of view, with a controlled step of 0.5°.

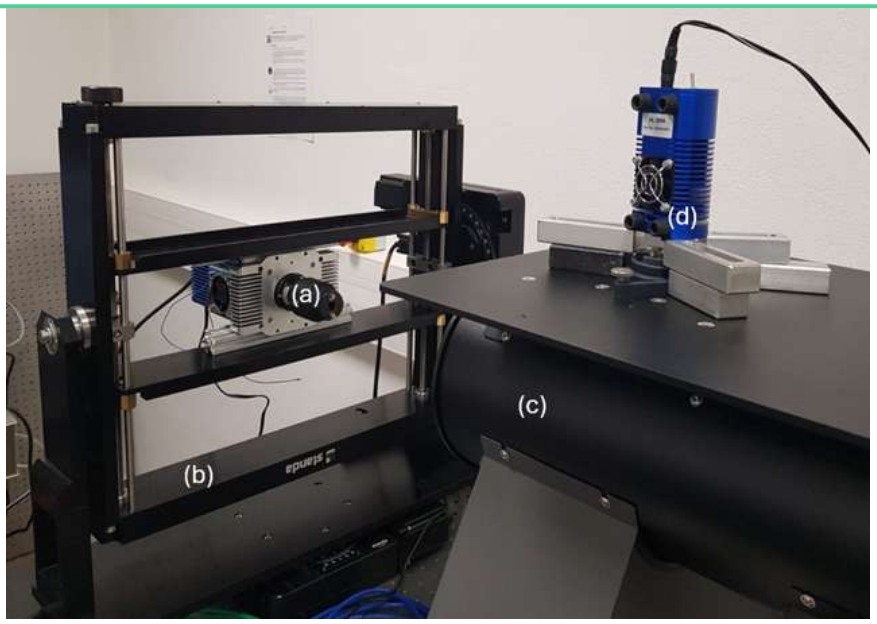

Figure 17/ Experimental setup (IPAG) used to measure the optical quality of NanoCarb-P (a) in the field of view. (b) goniometer; (c) collimator; (d) halogen source

3.3.2 Optical quality

We compute the Modulation Transfer Function (MTF) of the obtained images over three positions in the field of view, as shown on Figure 18.

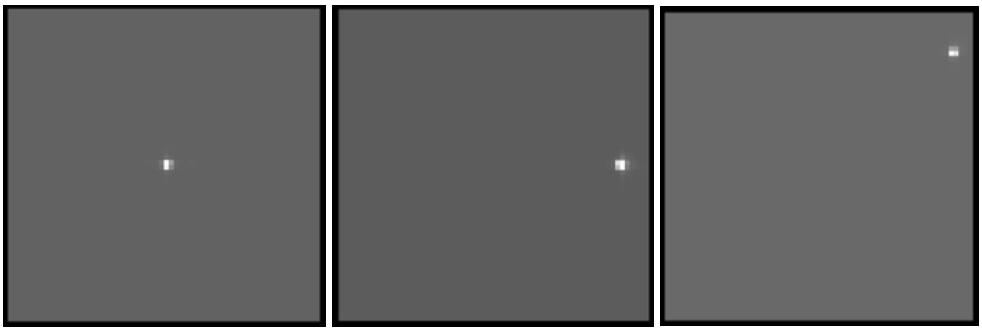

Figure 18: Point images obtained with the CO_2 camera in three positions of the field of view. From Left to right: centre of the field of view, right side, top-right corner

The MTF are plotted on Figure 19 for the CO2 camera and on Figure 20 for the CH4 camera. On the left column are plotted the MTF on the x axis, while y-MTF are plotted on the right. On each graph, the MTF for the 80 thumbnails are drawn. The spatial frequency of 1 corresponds to two times the Nyquist Frequency (end of the FFT window).

For all the investigated positions, and for the majority of the thumbnails, the optical quality is very high. Nevertheless, the PSF are sub-sampled (cutting frequency at 2 times the Nyquist frequency), that can induce some non-linear effects, especially when interpolating images to correct sub-pixel displacements, like during the L0 to L1 processing. This effect could be managed by blurring the images before interpolation.

For the CH4 camera, on the top right corner of field of view, we observe 5 thumbnails with a degraded MTF. This effect is probably induced by a vignetting effect of the image, only

affecting the corner of the field of view for the thumbnails on the border of the detector, with a neglectable impact over the performance.

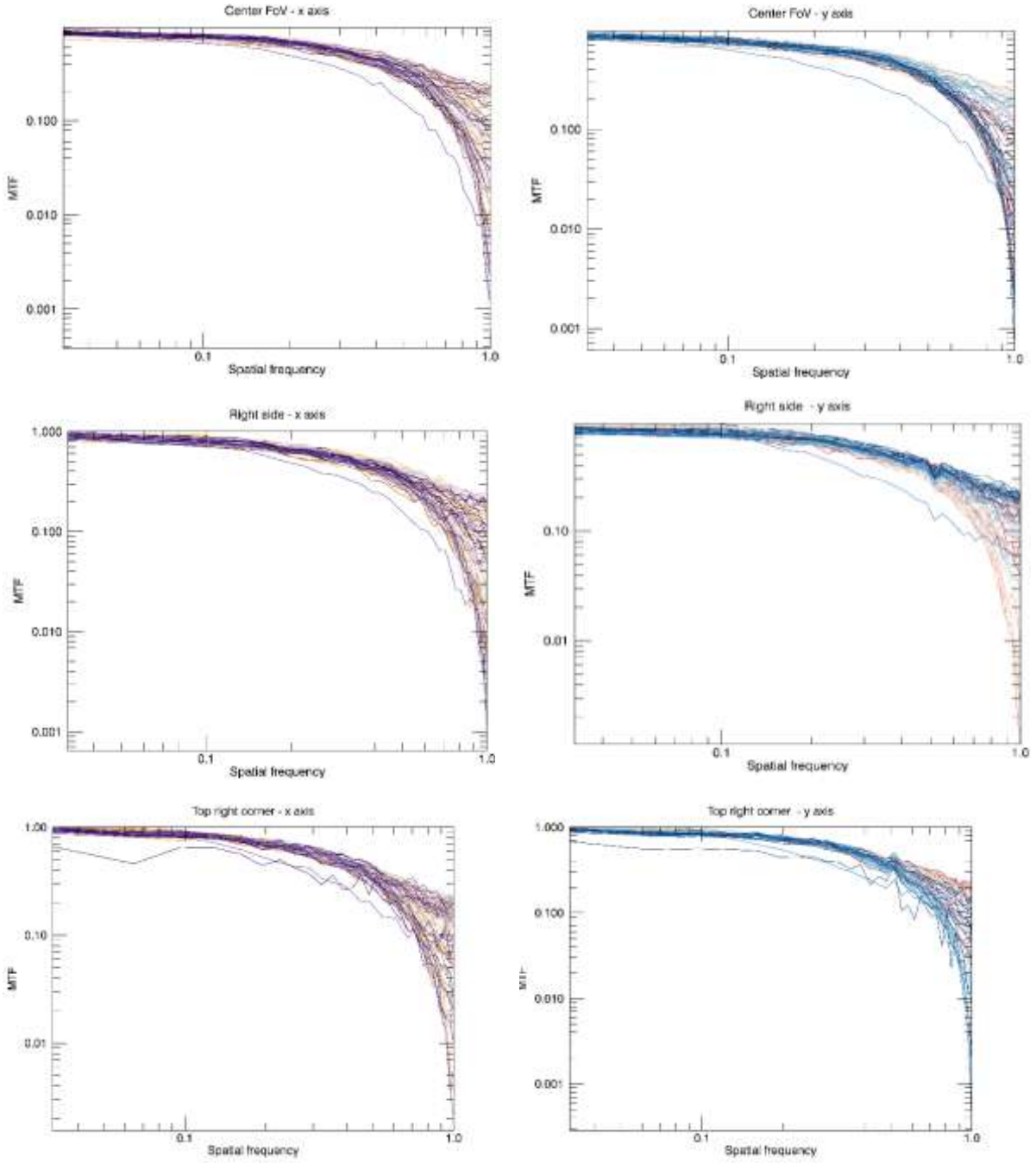

Figure 19: Modulation Transfer Function of the CO_2 camera.

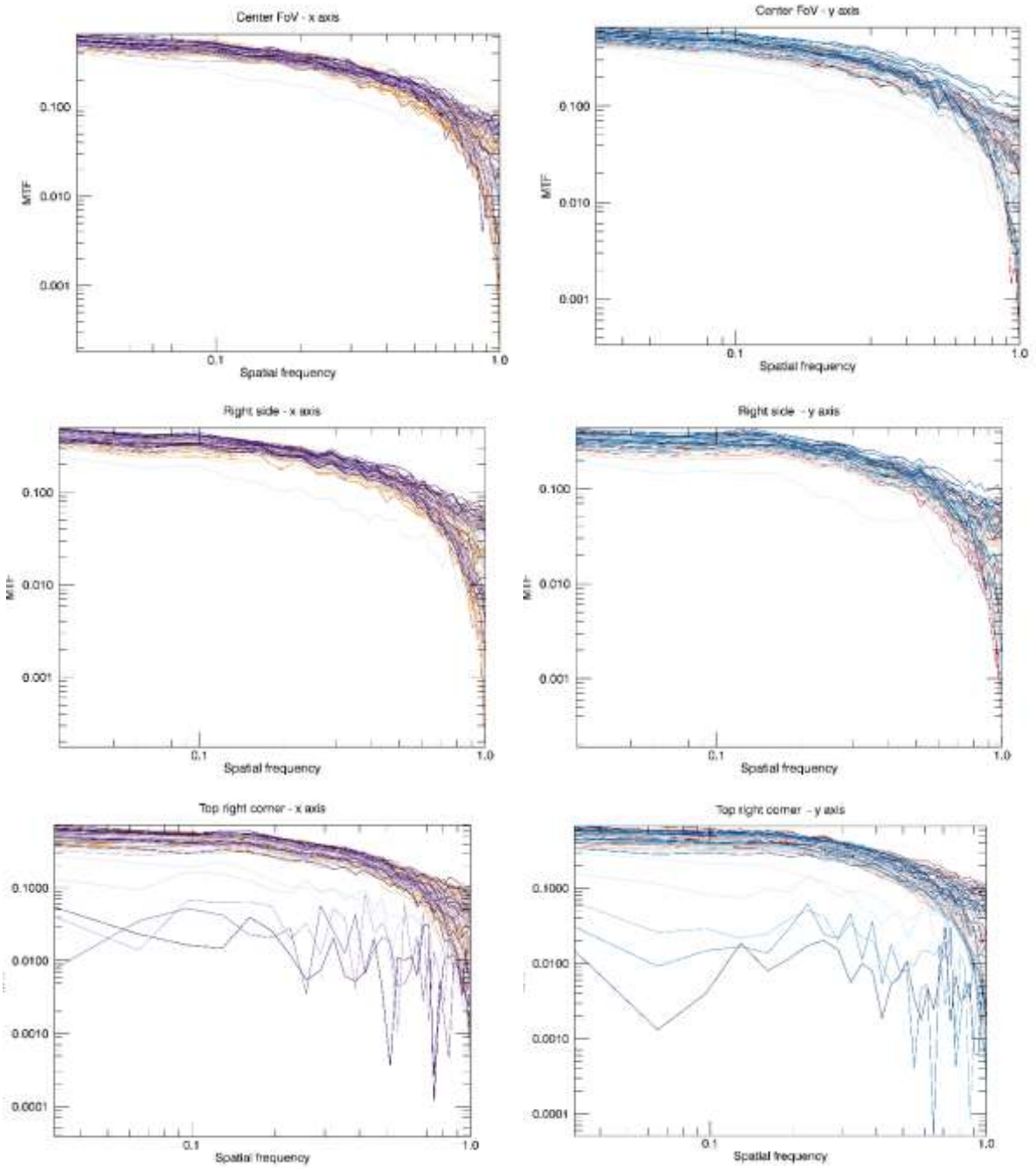

Figure 20: Modulation Transfer Function of the CH_4 camera.

3.3.3 Geometry and distortions

We investigate here the characterisation of the inter-thumbnail's distortions. This effect produces a sub-pixel displacement from one thumbnail to the other, that need to be corrected in order to reconstruct a proper interferometric cube (L1), by co-registering the thumbnails. To achieve this, we process all the images acquired during the spatial scan of the field of view. For each acquisition, we compare the position of the point image in all the thumbnails, referring to a reference thumbnail.

We build in that way a map of pixel displacement regarding this reference, as shown on Figure 21 for CO2 camera and Figure 22 for CH4 camera.

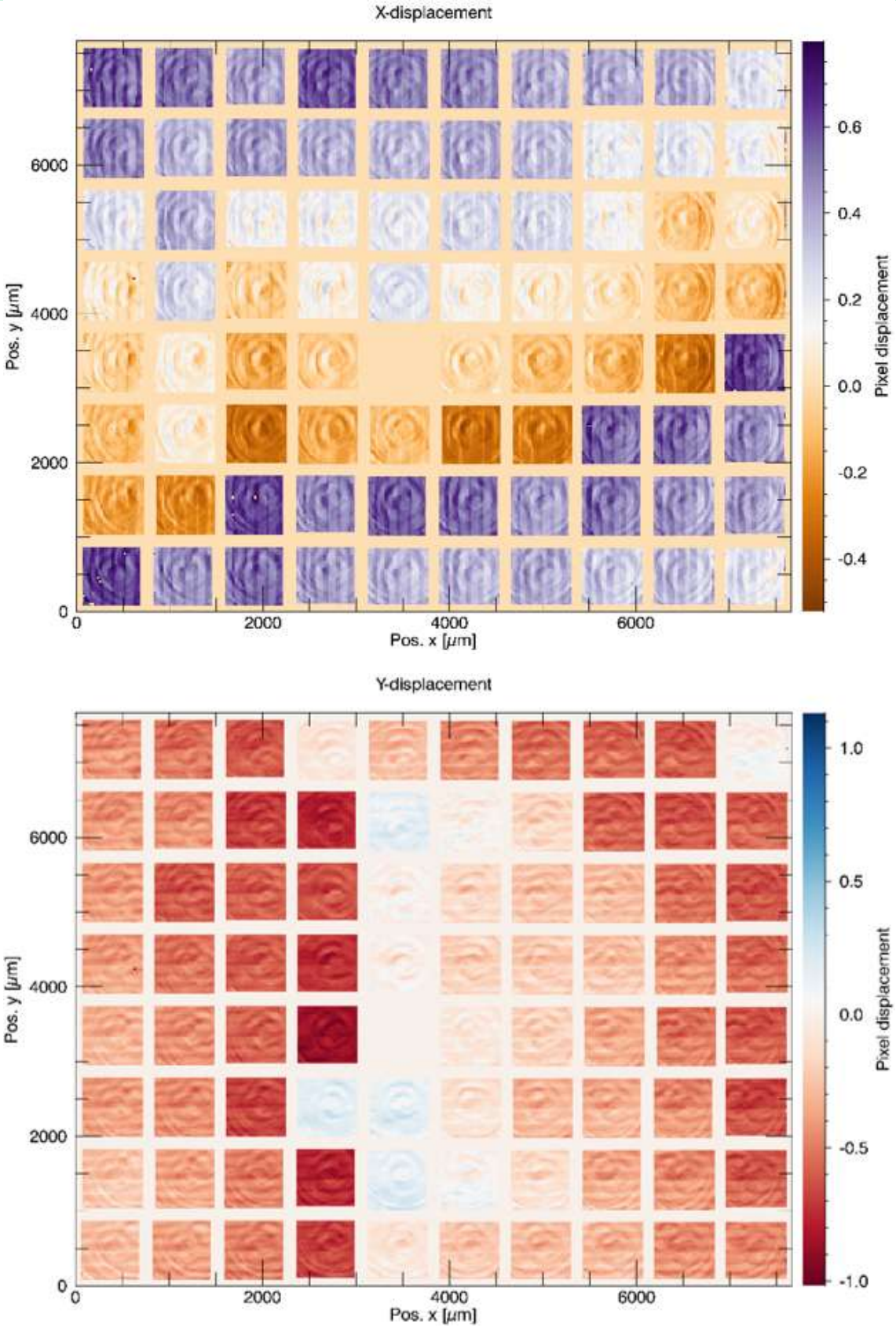

Figure 21: X and Y pixel inter-thumbnail displacements measured for the CO2 camera

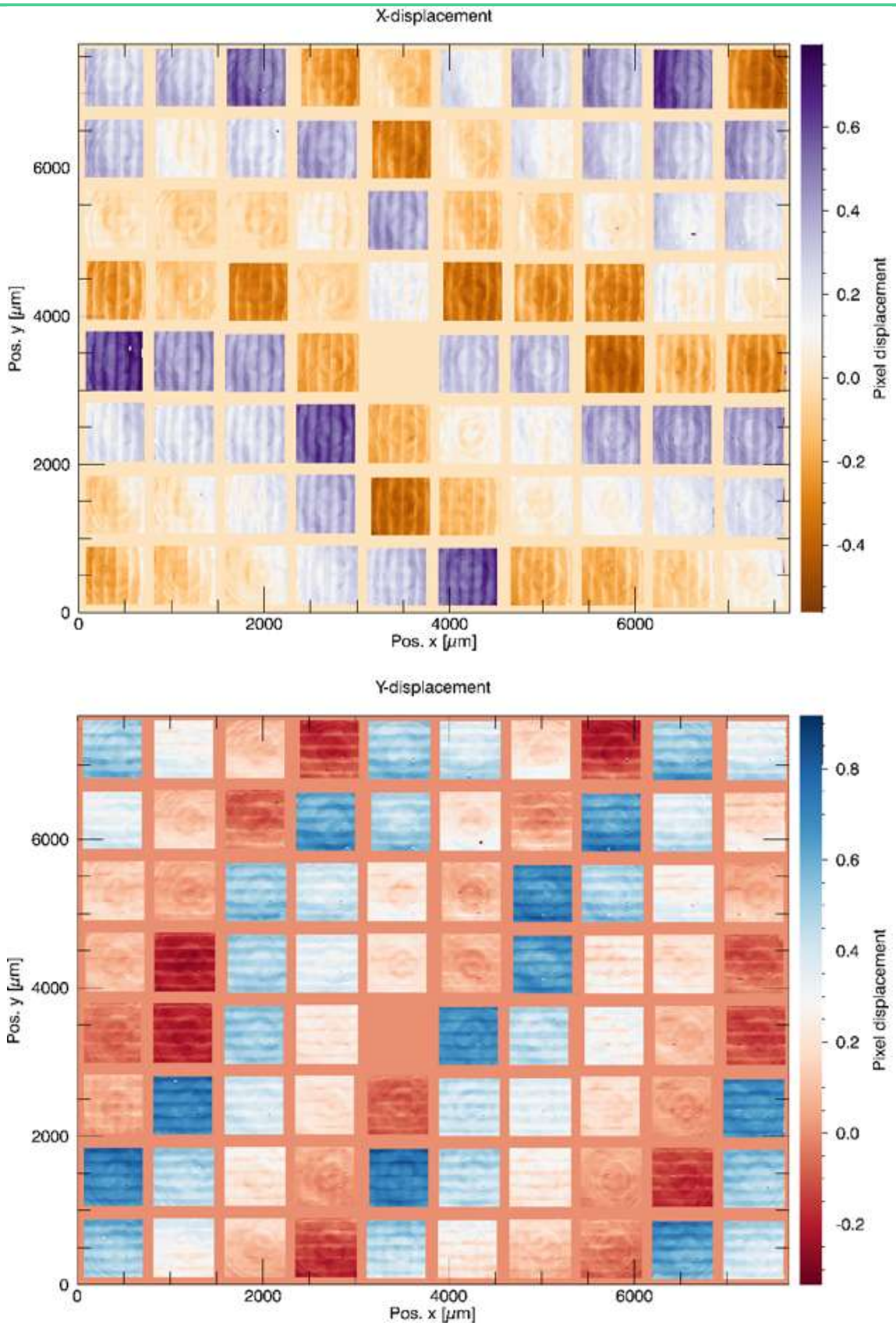

Figure 22: X and Y pixel inter-thumbnail displacements measured for the CH4 camera

In all the cases, the pixel displacements seem to be almost flat on each thumbnail, showing that the distortions are very small thank to the optical design of the objective.

The relative pixel displacement between thumbnails is consequently mainly a sub-pixel translation, due to some very small spatial unmatching between the pixel grid of the detector and the array of microlenses.

We observe also a sub-pixel fringing over each thumbnail. This effect is probably induced by the interpolation of the displacement computed at the positions of each point image. A bilinear interpolation instead a bicubic interpolation, as well as a blurring, could avoid this effect.

These maps are used in the L0 to L1 processing chain to co-register the thumbnails with a sub-pixel accuracy (see D5.1).

3.3.4 Ghost images

We started a preliminary analysis of the ghost images with NanoCarb-P cameras. At this point, it is just a comparison of the level of the main point image with the ghost. An example is shown on Figure 23.

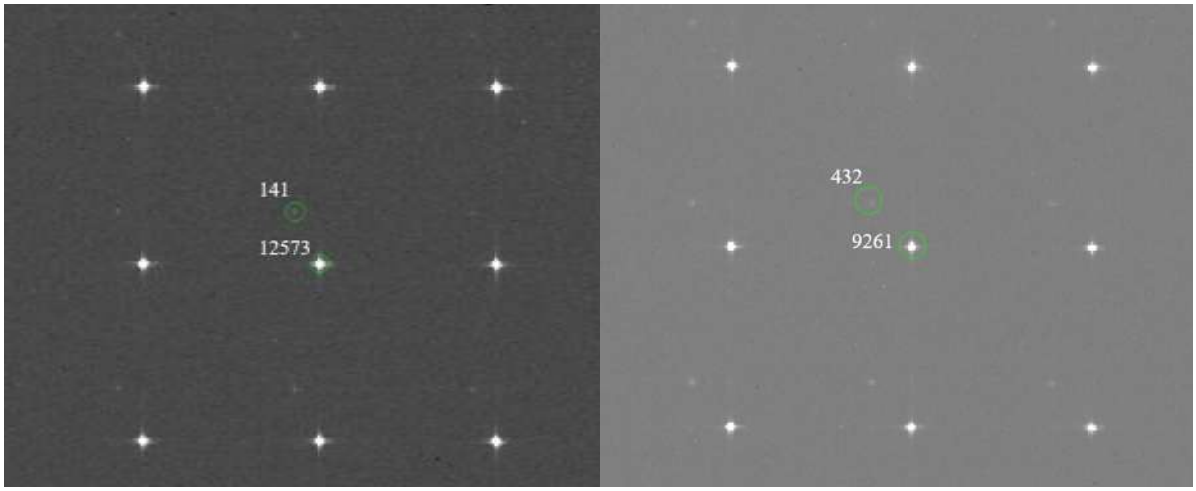

Figure 23: Example of ghost image captured for the CO2 camera (Left), and for the CH4 camera (Right). We compare the level of the main point image, with its ghost (in ADU unit)

The ghost images clearly appear for both CO2 and CH4 cameras:

- Ghost reflection ~1% for CO2
- Ghost reflection ~5% for CO2

These levels are slightly superior to the previous SCARBO prototypes, especially for the CH4 camera. This is probably a direct impact of the increase of the surface reflectivity of the interferometer, leading to internal parasitic reflection.

The impact is probably more important in terms on performances for the CH4 camera, especially for scenes with a high dynamic. The impact for the SCARBOn airborne campaign should remain low.

3.4 Spectral characterization

3.4.1 Objectives and methodology

We comment here the spectral characterization of NanoCarb:

- **Acquisition of the Instrumental Spectral Response Function (ISRF):** validation of the spectral modulation quality, combination of both the interferometric plate and the narrow-band filter responses, ensuring performances as specified. The ISRF is also crucial to process the data from L1 to L2, using in addition radiometric calibrations.
- **Radiometric calibration** is also essential, to correct pixel non uniformities taking into account both pixel response and optics in front.
- **ISRF stability**: test of the stability of NanoCarb-P before and after the scientific flight.

The ISRF is acquired using a monochromatic scan within homogeneous illumination. The camera is placed in front of an integrated sphere, providing such a homogeneous illumination of the field of view of NanoCarb. We use a tuneable laser, coupled to a wavemeter in order to precisely control the wavelength of the source. An image is acquired for each step of the laser, within the range of sensitivity of the CO2 or CH4 camera. A power meter provide a reference of the optical power in parallel of the acquisitions. The experimental setup is shown on Figure 24. This setup was deployed during the campaign just before the integration of NanoCarb in the aircraft, then just after dismounting, in order to provide calibration data as close as possible from the scientific flight.

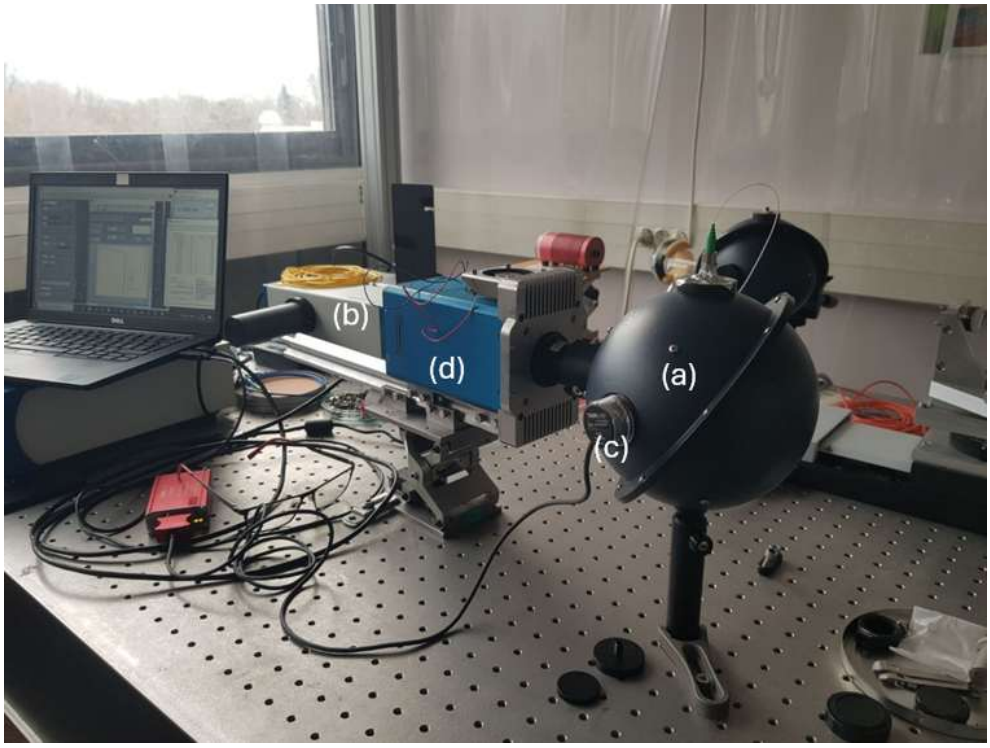

Figure 24: Experimental setup (IPAG) used to measure the ISRF of NanoCarb (d). (a) integrating sphere: (b) tuneable laser; (c) power meter. A wavemeter is also used in parallel

Radiometric calibration is provided by ONERA, using an integrating sphere coupled to a wide band source radiometrically calibrated. Acquisitions are made at several exposure times, to compute a pixel radiometric gain map.

3.4.2 Instrumental Spectral Response Function (ISRF)

- **CO2 camera:**

On Figure 25, we compare for a single pixel the spectral response before and after coating. We clearly observe the increase of the modulation contrast due to the increase of surface reflectivity (from ~33% for native silicon to 55% in NanoCarb-P).

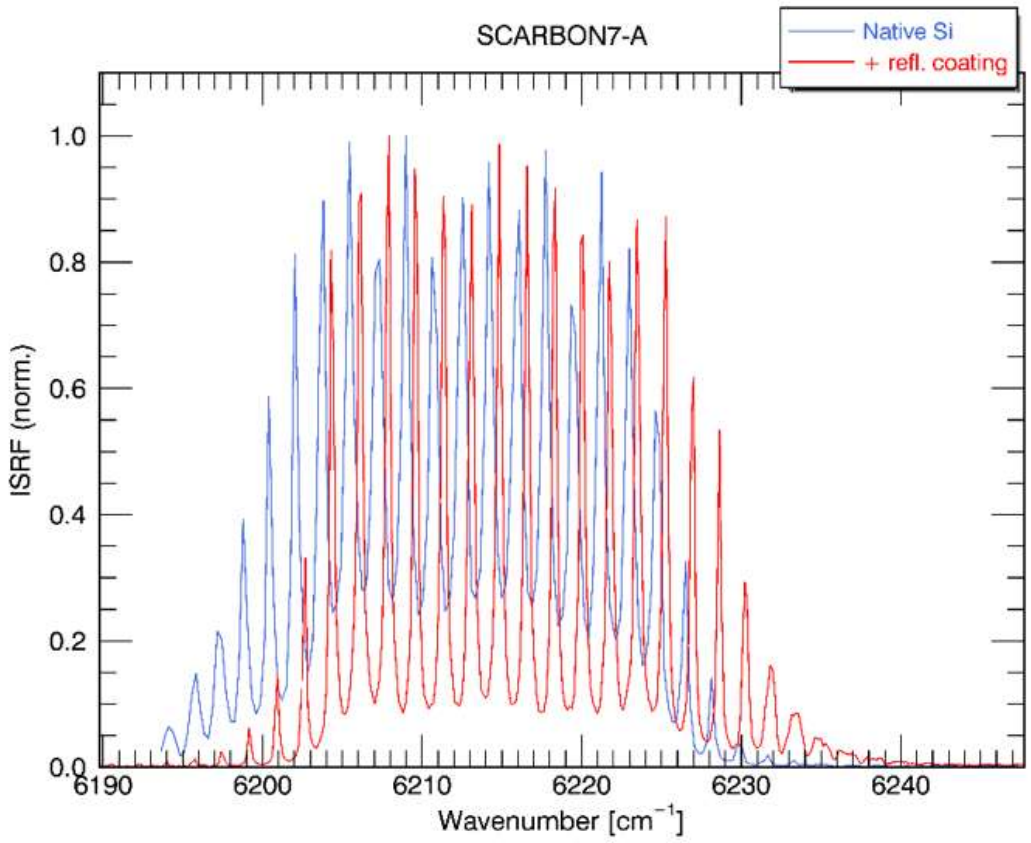

Figure 25: CO2 single pixel's ISRF comparison before and after coating of the interferometer

On Figure 26, we show an illustration of the ISRF acquisition for the CO2 camera. On the left, a picture of a single acquisition at 1610.9 nm from the scan, at the centre of the spectral bandwidth. We observe well contrasted Fabry-Perot rings as expected, without warping or distortions (potentially induced by a misalignment between the microlenses and the interferometric plate).

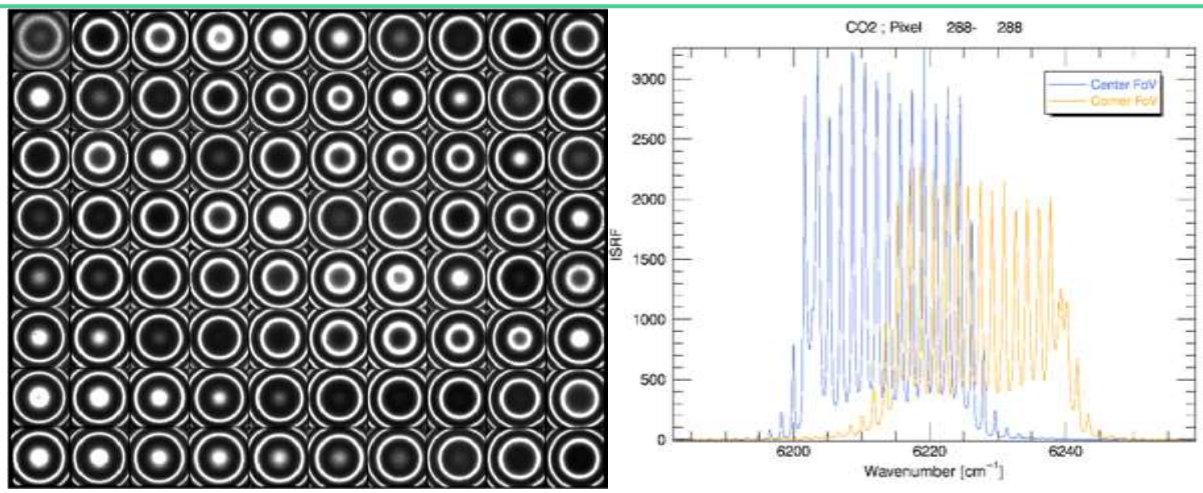

Figure 26: Left: single acquisition of the monochromatic scan of the CO2 camera at 1610 nm. Right: single pixel ISRF comparison between the centre and the corner of the field of view

We notice on the top-left a thumbnail with less contrasted rings. This is the already identified thumbnail, where the interferometric plate shows a defect (see 2.2.4).

On the right of the figure, we draw a comparison between the spectral response of two single pixels, the first on the centre of the field of view, and the second on the corner. We observe in this case a decrease of both the transmission and of the contrast in the corner, regarding the centre of the field of view. This effect is due to the narrow-band filter integrated in the CO2 camera, presenting an important spectral shift with the angle of incidence.

- **CH4 camera:**

On Figure 27 we draw the comparison for CH4 between ISRF at the centre of the field of view in blue, to the corner in orange. We observe in this case a very small shift of the spectral band, thanks to the high index narrow-band filter characterized above. The contrast of the fringes is also increased regarding native silicon, as expected with a surface reflectivity close to 78%.

Nevertheless, some peaks appear as doubled. This effect is probably caused by internal parasitic reflections, as previously investigated. This effect is lower on the CO2 camera and appears only on the wings of the spectral band as visible on Figure 28 on the left of the band.

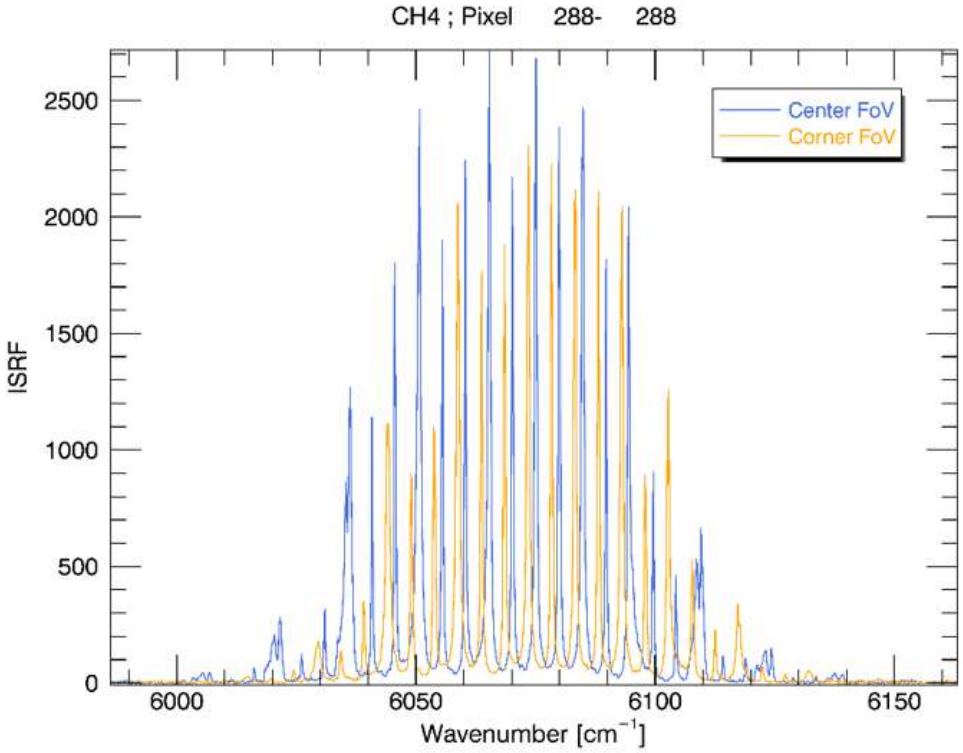

Figure 27: CH4 single pixel ISRF comparison between the centre and the corner of the field of view

3.4.3 ISRF comparison before and after the campaign

We compare on the Figure 28, the ISRF acquired the 30th of March 2026 in Barcelona, just before NanoCarb integration, to the acquisition after dismounting the 10th of April.

Based on this single pixel example, the two ISRF seems to be very close. Some amplitude variations may be noticed but are mainly caused by a sampling effect. We do not observe phase shift or variation of the global shape.

The main issue concerns the doubled peak on the left-wing of the band. We suspect an effect of an internal reflection, slightly varying during the campaign due to a very faint shift of position of the optical elements. Direct simulations show a neglectable impact over the interferogram modelling and thus over the performances.

The NanoCarb-P ISRF seems to be stable at this scale.

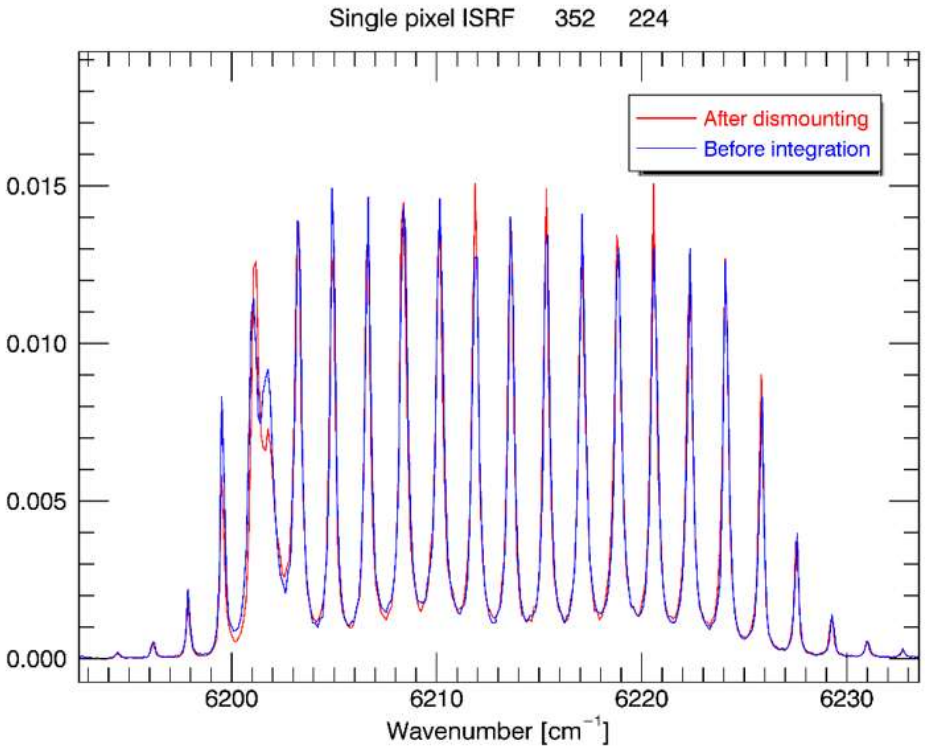

Figure 28: CO2 single pixel ISRF comparison before and after the campaign

3.4.4 Radiometric calibration

The radiometric calibration allows to derive a radiometric gain map, which is essential to convert the signal into radiometric unit, usable in physical retrieval model, then to correct pixel non-uniformities. The obtained CO2 map is presented on the Figure 29.

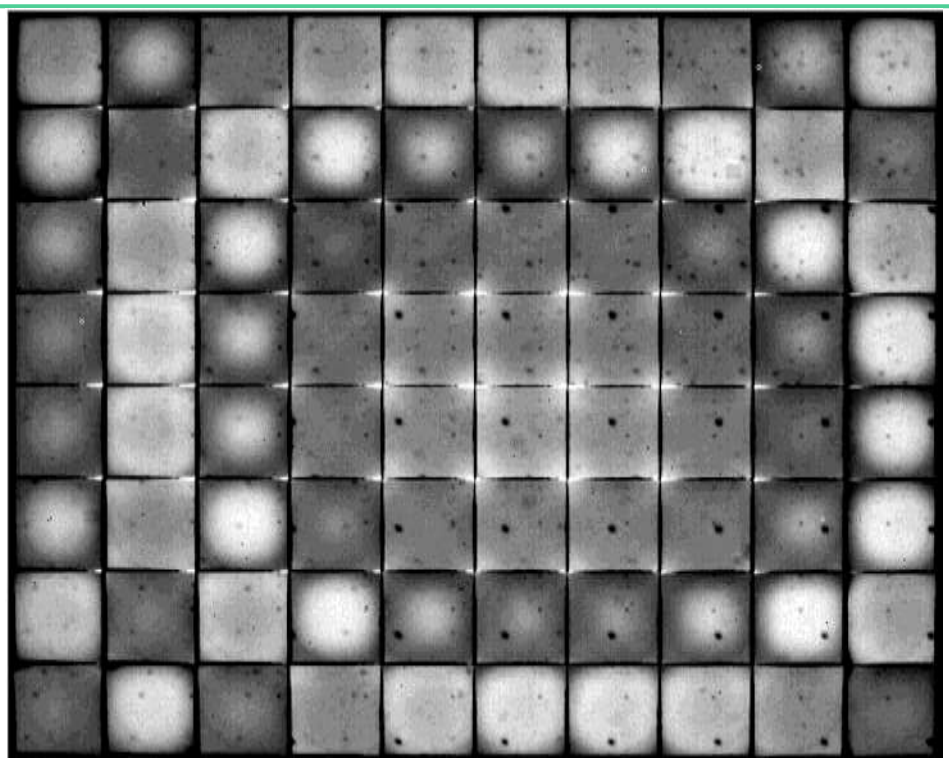

Figure 29: CO2 radiometric gain map [ADU/(ph.m².strd)]

The Figure 30 makes apparent transmission variation in the field of view of the thumbnails, induced by the narrow band filter.

We observe also a lot of dusts over the optics. The repetition of the same pattern of dust over all the thumbnails shows probably that these dusts are localized over the front optics, seen by all the sub-apertures.

This map *Rad* is used as a flat field correction during pre-processing of L0 raw data as following:

$$L_0^{corr} = \frac{L_0 - dark}{Rad \times ti}$$

With L_0^{corr} in Photon/(s.m².strd), and *ti* the exposure time.

3.5 Detector dark current characterization

Dark signal characterization has been already achieved by ONERA during the first SCARBO project, with exactly the same detectors. We focus here on the calibration datasets acquired shutter closed before and during the campaign, as they are essential in the data processing chain from L0 to L1.

Several batches are available, from laboratory calibration at ONERA, to acquisitions during the campaign, at the ground once the instruments have been integrated on the aircraft, then during the scientific flight before the arrival above the powerplants.

Median level over the detector as a function of the exposure time is presented on the Figure 30. Exposure time during the flight was 15 ms. We clearly identify over the graph some variation of the dark signal, between 2 and 5 ADU, very close to the calibration in laboratory.

On the Figure 31, we assess the impact of these variations over the L1 extracted interferograms. Observed differences between the curves, corresponding each to a different dark acquisition, are very faint, demonstrating a neglectable impact over the signal, and thus over the performances.

This dark signal stability is consequently satisfactory enough for the airborne campaign.

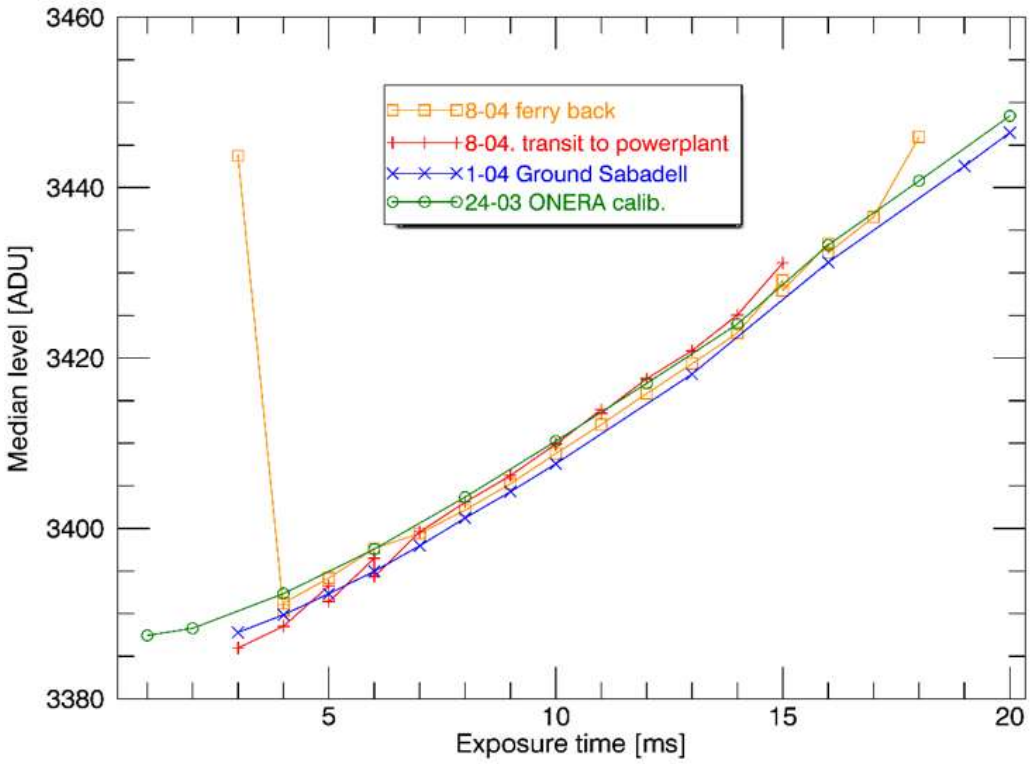

Figure 30: CO2 dark median level over the detector as a function of the exposure time. Comparison between the different sets of calibration

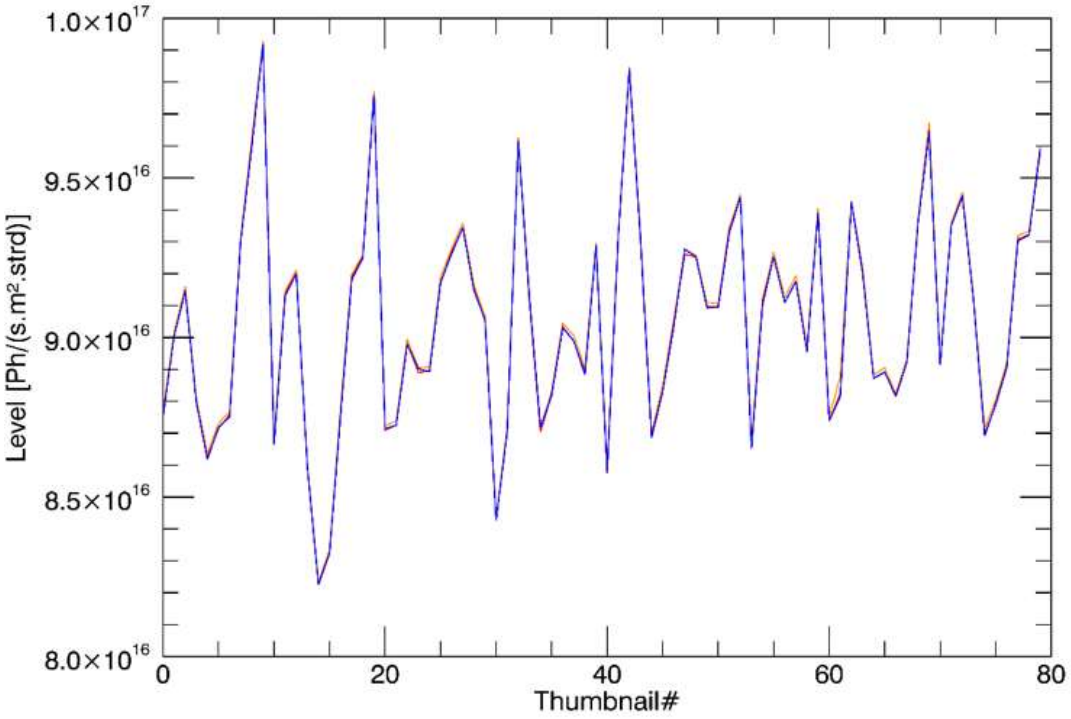

Figure 31: CO2 interferograms comparison by using the different batches of dark

4 NanoCarb-P thermal testing

4.1 Introduction

This section describes the thermal investigation conducted by Absolut System to improve the performance of the NanoCarb cameras. During a previous airborne campaign, it was observed that the NanoCarb cameras were not able to provide sufficient self-cooling under certain environmental conditions, leading to degraded thermal performance.

Absolut System is responsible for the implementation of the thermal performance improvements, which are detailed in the following sections.

4.2 NanoCarb-P camera initial performance

The results presented in this sub-section correspond to the initial thermal performance characterization of the SCARBO prototype cameras. These tests were conducted as part of the prototype development activities and provide a baseline assessment of the thermal behaviour of the camera system in its original configuration.

The test campaign was performed before the hardware upgrade and prior to the integration of the new optical components introduced in the updated design. Consequently, the results presented here reflect the performance of the cameras in their original configuration and should be considered as a reference for the subsequent improvement and optimization of the SCARBOn prototypes.

The data obtained from these tests were used to evaluate the thermal stability of the system, identify potential areas for improvement, and support the design evolution that led to the current SCARBOn camera configuration. As such, the results provide valuable insight into the performance of the initial prototype and establish a benchmark against which the effectiveness of later design modifications can be assessed.

4.2.1 CO2 camera

Initially, the CO2 camera operating capabilities are summarized in Table 3.

Operating scenario	Temperature
Maximal operating temperature	26°C
Minimal operating temperature	14°C

Table 3: Initial operating temperature range of the CO2 camera

Test results showed that the CO2 camera was able to operate under ambient conditions up to 26°C. Beyond this temperature, the Peltier system reached its regulation limit. Although the control loop remained active, the system was unable to further decrease the optical temperature. As a result, the required thermal setpoint could not be maintained at higher ambient temperatures, which directly impacted the camera performance.

4.2.2 CH4 camera

Initially, the CH4 camera operating capabilities are summarized in Table 4.

Operating scenario	Temperature
Maximal operating temperature	22°C
Minimal operating temperature	14°C

Table 4: Initial operating temperature range of the CH4 camera

The CH4 camera demonstrated low performance across the tested temperature range.

The Peltier system showed limitations in maintaining the required temperature setpoint under elevated ambient conditions. The optical subsystem temperature was observed to be strongly correlated with the ambient temperature, indicating insufficient thermal regulation.

More specifically, the optical temperature increased proportionally with the ambient temperature, demonstrating that the TOC system was not able to maintain stable control at higher temperatures. This behaviour suggests that the Peltier system had limited cooling capacity or was not operating at its nominal performance.

4.3 NanoCarb-P camera hardware upgrade

4.3.1 Thermal conductivity enhancement

During CH4 camera dismounting, it has been found that there was a gap between the Peltier hot side and the camera front panel. This impacts significantly the thermal dissipation of the Peltier reducing the cooling efficiency.

Hence, a 150 µm thick copper layer has been inserted to fulfil this gap. As shown on the following figure, the copper layer is directly on the front panel side.

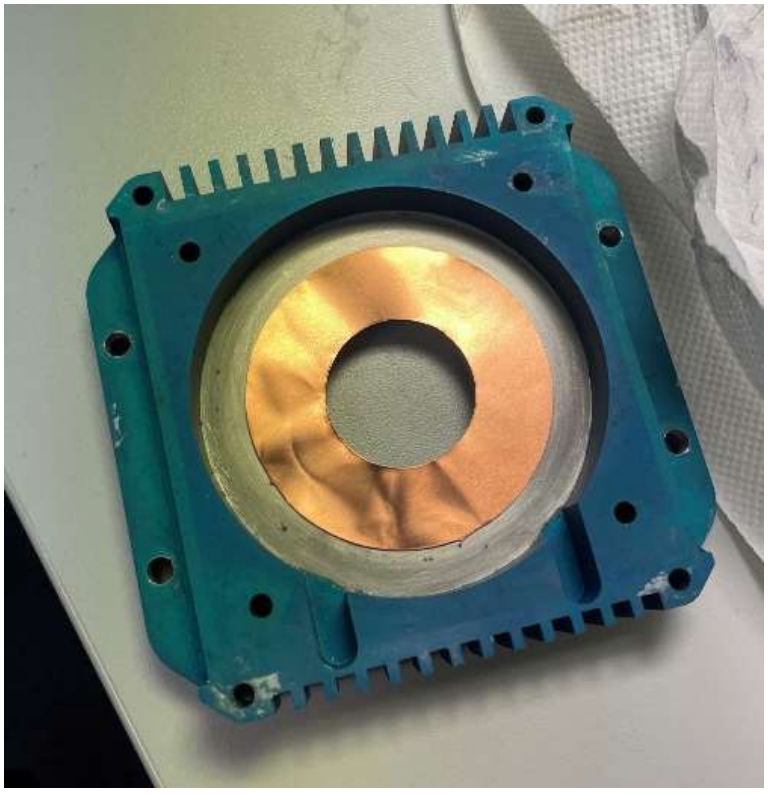

Figure 32: CH4 Font camera panel with the copper layer

To enhance the thermal dissipation, a heatsink with high thermal conductivity (Table 3) has been used. It has been applied to all thermal interface such as Peltier cold and hot side and camera front panel. The heatsink has the following properties:

Parameters	Value	Unit
Name	Thermal Grizzly Kryonaut	-
Model	TG-K-001-RS	-
Thermal conductivity	12,5	W/mK
Operative temperature	-200 to +350	°C
Electrical conductivity	No	-

Table 5: Heatsink properties

The heatsink is applied between all new components enhancing the thermal conductivity.

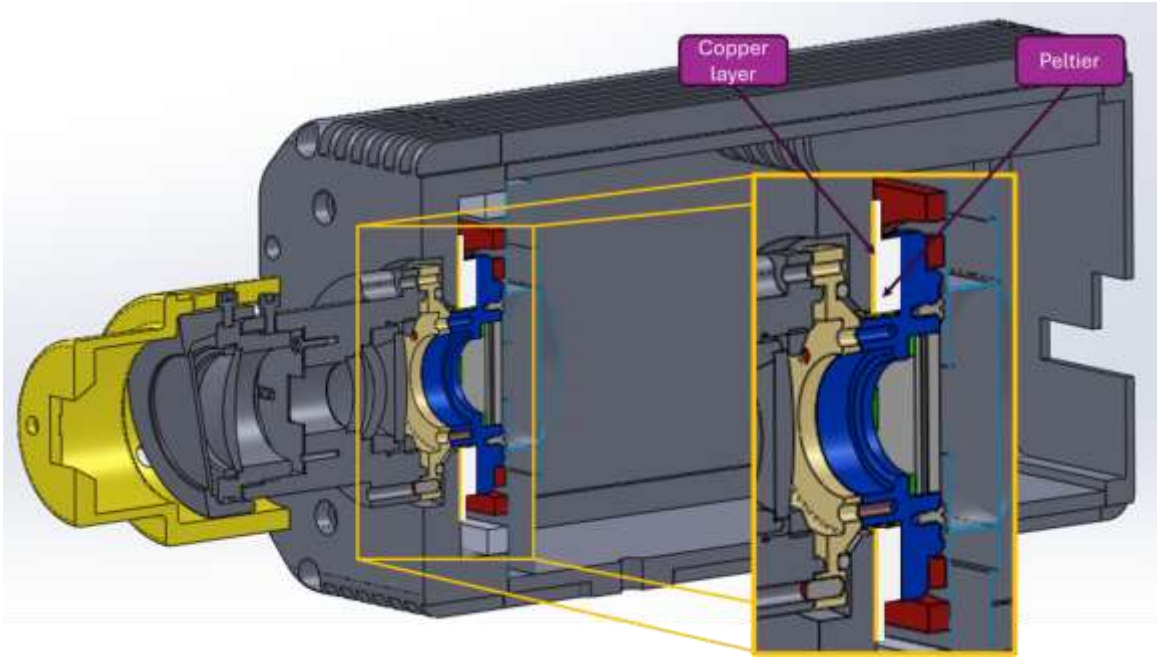

Figure 33: Thermal conductivity enhancement detail

4.3.2 Front panel design

To increase the heat dissipation a new aluminium 6061 (Table 6) front panel has been designed and assembled on both cameras. These panels are larger than the original ones and have a shape with a higher surface area (it corresponds to the wing visible in Figure 34, which enhance heat dissipation. Moreover, fans are mounted on both sides of the panels to increase the heat dissipation by forcing the convection of the front panel heat. The fans only have 2 electrical pins (- and +) which are not connected to the camera which means that they require a dedicated external power supply.

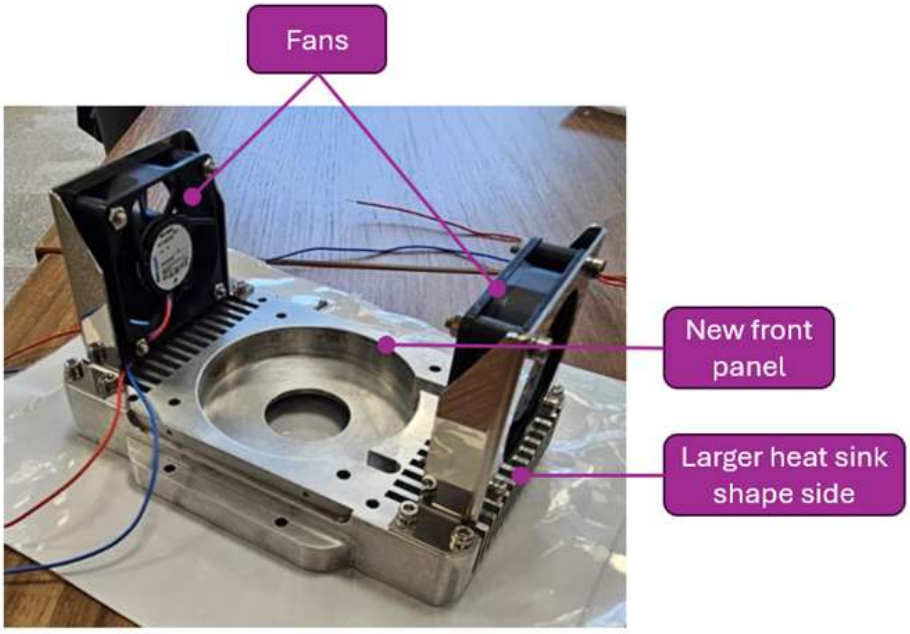

Figure 34: Front panel with the two fans mounted

Parameters	Value	Unit
Name	Aluminium 6061	-
Thermal conductivity	152	W/mK

Table 6: Front panel material characteristics

4.3.3 Peltier module

During cameras operations, it has been found that:

- The **CH4 Peltier** has slightly melted due to low heat dissipation leading to lower cooling performance.
- The **CO2 Peltier** has been damaged during the integration of a new optical filter which significantly reduced its cooling performance. Indeed, after the filter integration on the CO2 camera, the Peltier could not cool the optical components in ambient conditions.

Hence, those Peltier have been replaced by new ones which allowed to reach higher performances than the previous configuration. The following table depicts the characteristics of the new Peltier module.

Parameters	Value	Units
Ceramic material	Al2O3	-
Qc (ΔT=0)	12,4 (@27°C)	W
ΔTmax (Qc=0)	70,5 (@27°C)	°C
Max operating temperature	80	°C
Weight	20,0	g

Table 7: Peltier characteristics

4.4 Test setup and instrumentation

4.4.1 Climatic chamber description

To control and simulate the NanoCarb-P environmental conditions, a Binder MKFT720 climatic chamber was used. This chamber allows precise control of both temperature and humidity throughout the test campaign.

4.4.2 Test bench description

Both NanoCarb-P cameras (CH4 and CO2) were installed inside the climatic chamber. In order to better characterize thermal variations, additional temperature sensors were installed on the front face of each camera.

To support the additional cooling requirements, an external fan system was implemented as detailed in section 4.3.2. A dedicated power supply was designed to provide electrical power to the fans. Each fan input is connected via a dedicated connector, with identical connectors used for both input and output interfaces.

The fans are powered by an external power supply delivering 24 V, with a nominal current consumption of 39 mA, in accordance with the manufacturer's specifications. For the airborne campaign, this power supply will be provided through a single harness connected to the fan via a TE M8 connector.

The following test bench was implemented for the thermal test:

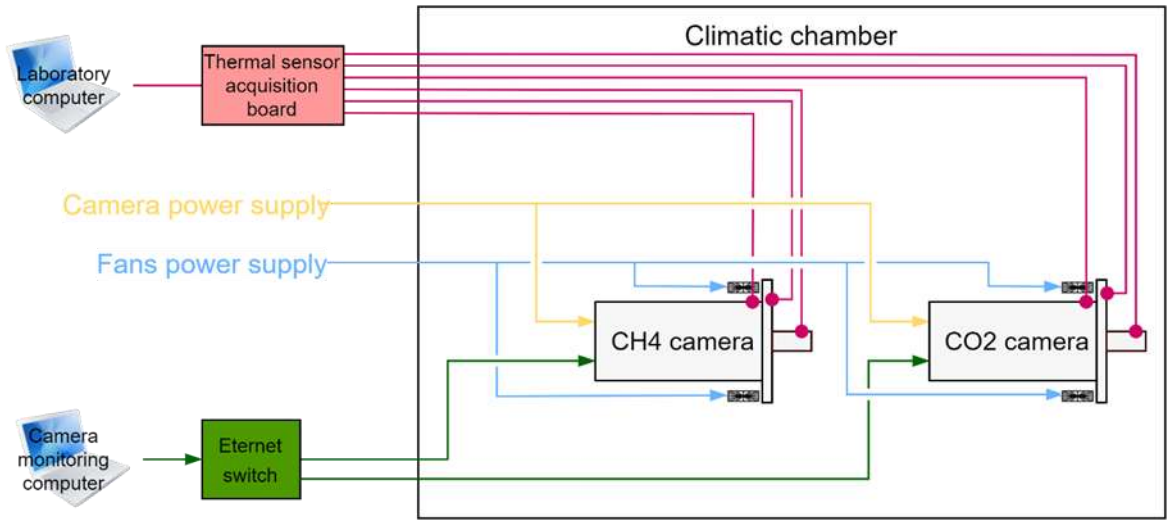

Figure 35: NanoCarb test bench

4.4.3 Instrumentation description

Three additional temperature sensors were installed on each camera:

- One sensor on the **front panel** (1) to evaluate heat dissipation.
- One sensor on the **optical ring** (2) to monitor local temperature variations.
- One sensor on the **telescope structure** (3).

These sensors were implemented to assess the effectiveness of the thermal control system, specifically to verify the heat dissipation from the Peltier hot side and to validate the hardware modifications.

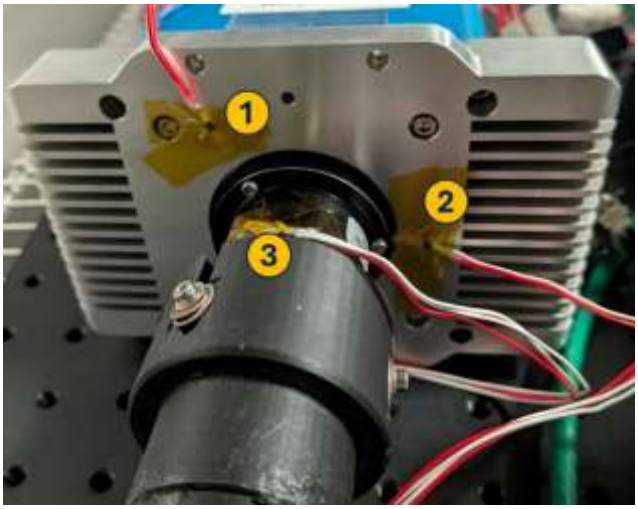

Figure 36: Location of thermal sensors

4.4.4 Camera control description

Both the CH4 and CO2 cameras were controlled and monitored via an Ethernet interface. An Ethernet switch was used to connect both cameras to a single control computer, enabling simultaneous operation and data acquisition.

4.5 Test conditions

To confirm the NanoCarb camera performance under controlled environmental conditions, a temperature plateau test strategy was implemented, as illustrated in Figure 37.

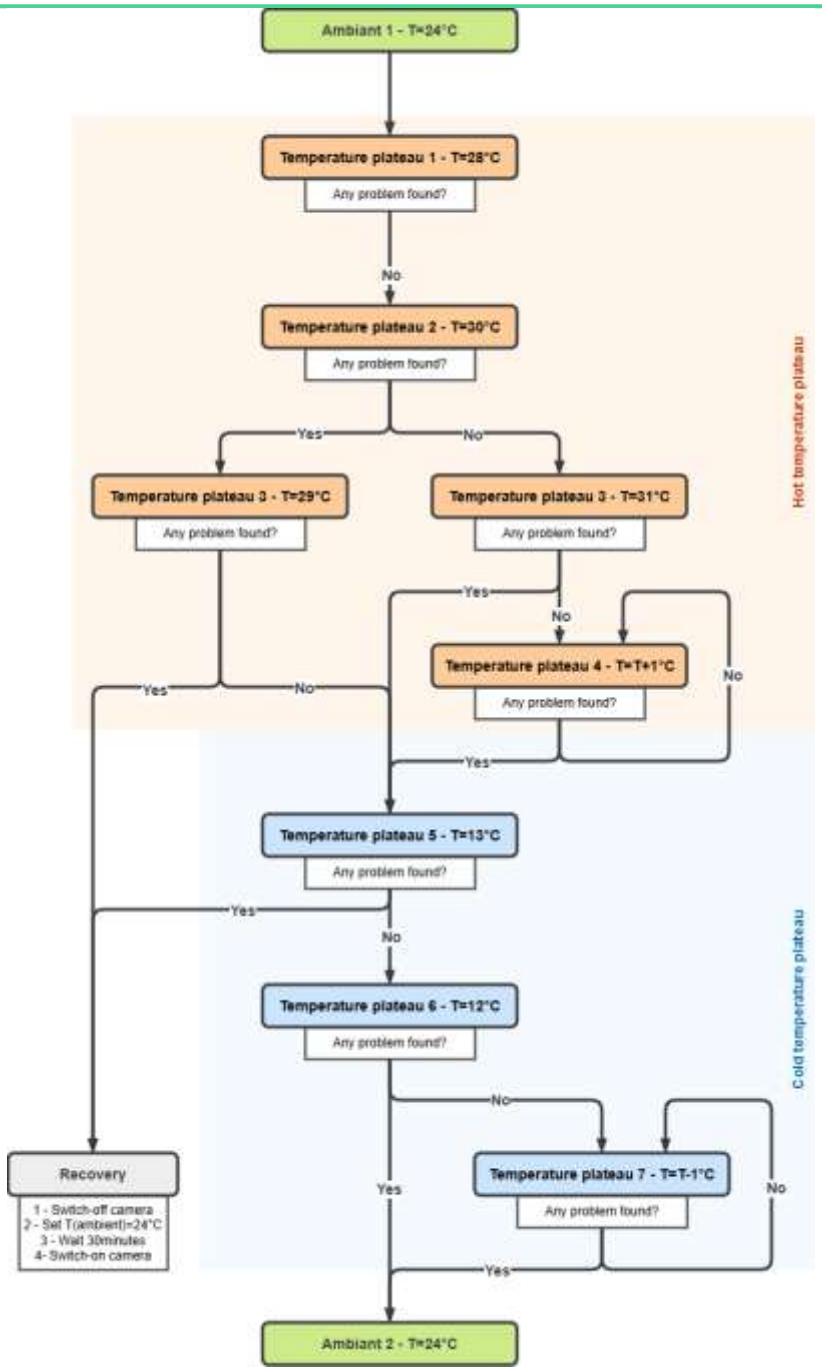

Figure 37: Thermal test investigation strategy flow

The test campaign consisted of successive temperature plateaus, both at high and low temperatures, in order to evaluate the operational limits of the cameras. At each plateau, the system was allowed to reach thermal stabilization before assessing the camera performance. For each temperature plateau, the following test sequence was applied:

- A stabilization period of **30minutes** was maintained to monitor the thermal behaviour and temperature variation of the NanoCarb-P cameras.
- This was followed by two power cycling sequences (switch-off / switch-on), each including a stabilization period of **5minutes**, in order to confirm the camera behaviour and robustness during rapid restart conditions and allowing sufficient duration to the temperature to stabilize.

The test sequence was performed iteratively for both hot and cold conditions, with the objective of determining the maximum and minimum ambient temperatures at which the cameras can operate nominally.

In the event of a test failure (e.g., inability to reach or maintain the required setpoint, or loss of functionality), a recovery procedure was applied. This procedure consists of:

- Switching off the camera.
- Reducing the ambient temperature to 24 °C.
- Waiting for thermal stabilization.
- Switching the camera back on and verifying nominal operation.

This recovery sequence was implemented to ensure safe test continuation and to evaluate the camera restart capability after thermal stress.

4.6 Results and analysis

4.6.1 CH4 Camera

To compare the initial and final performance of the CH4 camera at an ambient temperature of 28°C, the temperature evolution and Peltier current were monitored, as shown in the following figure.

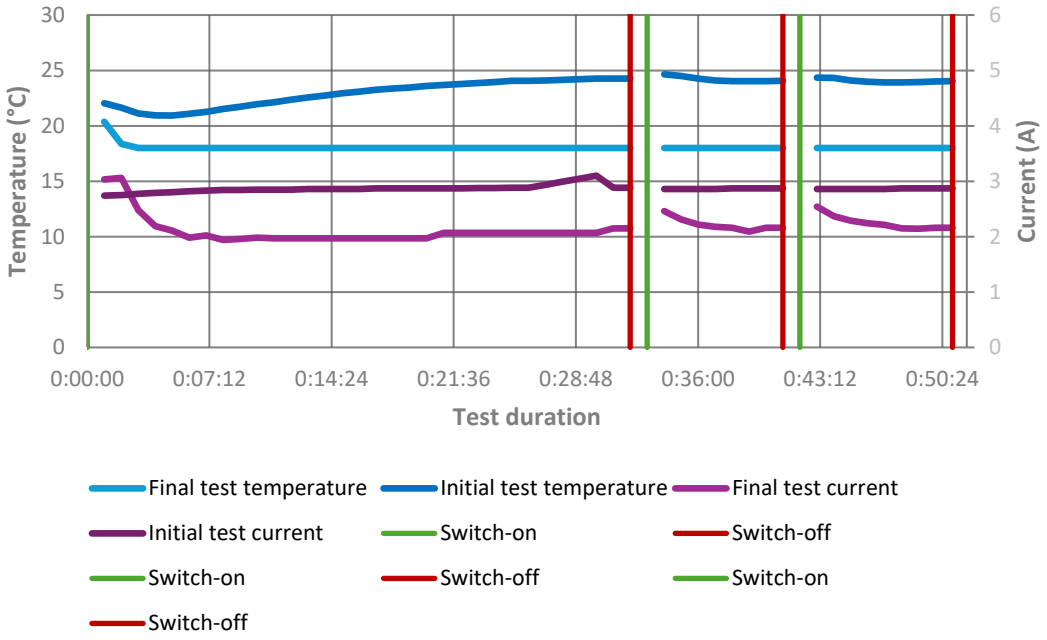

Figure 38: CH4 camera initial and final test parameters variation

During the initial test, the target temperature was set to 18°C. However, the Peltier system was not able to reach this setpoint. The temperature initially increased and then stabilized around 24°C, corresponding to a temperature difference of +6°C with respect to the target

and only a 4°C margin relative to ambient conditions. This indicates limited cooling performance of the thermal control system.

In contrast, during the final test, the Peltier system reached the 18°C target temperature immediately and maintained it within a ±0,1°C margin. In addition, the Peltier current decreased to approximately 1A, indicating improved thermal efficiency.

These results demonstrate that the implemented hardware has significantly improved the thermal control performance of the CH4 camera, both in terms of operative temperature and power consumption.

4.6.2 CO2 Camera

To compare the initial and final performance of the CO2 camera at an ambient temperature of 28°C, the temperature evolution and Peltier current were monitored, as shown in the following figure.

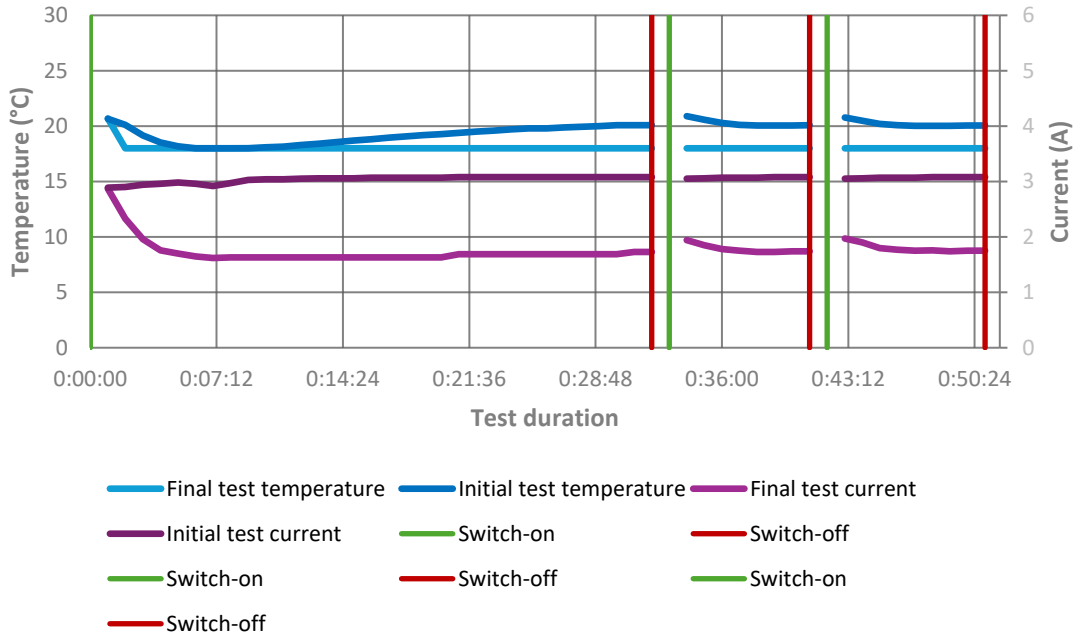

Figure 39: CO2 camera initial and final test parameters variation

During the initial test, the target temperature was set to 18°C. The temperature of the optical module stabilized around 19,5°C, indicating that the required setpoint was not achieved. This corresponds to a temperature difference of 1,5°C compared to the target and approximately 8,5°C with the ambient temperature, highlighting a limitation in cooling capacity. This behaviour implies that the CO2 camera was able to regulate temperature only up to an ambient condition of approximately 26,5°C (i.e., 18°C + 8,5°C).

Following the hardware upgrades, the Peltier system successfully reached the 18°C target temperature and maintained stable regulation. In addition, the Peltier current was reduced to approximately 40% of its initial value, demonstrating improved efficiency and thermal performance.

These results confirm that the hardware modifications significantly enhanced the CO2 camera thermal control capability.

4.7 Conclusion

The thermal test campaign following the hardware upgrades demonstrated a significant improvement in the operating temperature range of both NanoCarb cameras.

NanoCarb-P CH4	Initial test	Final test
Max. operating temperature	22°C	29°C
Min. operating temperature	14C	10°C

Table 8: CH4 camera operating range

NanoCarb-P CO2	Initial test	Final test
Max. operating temperature	25°C	30°C
Min. operating temperature	14C	9°C

Table 9: CO2 camera operating range

Both cameras show an extension of their operating temperature ranges, with improvements observed on both the upper and lower operational temperature.

Thus, the achievable operating range is extended up to 20°C ± 10°C, demonstrating a significant increase compared to the initial performance.

The upgraded thermal control systems are therefore expected to ensure stable and reliable operation of both cameras under the environmental conditions anticipated during the airborne campaign.

5 Conclusion

This document reports the results of the optical component characterization, detector and optical integration tests, and thermal tests at system level.

The interferometric plate characterization demonstrates optical quality for both the CO2 plate and the CH4 plate. The reflective coating characterization shows that the transmission peak exceeds the specification by 14% for the CO2 plate and by 35% for the CH4 plate.

The qualification activities confirmed that the instrument performance is consistent with mission requirements. Any observed deviations from the target specifications are minor and remain within acceptable operational limits.

The detector dark current is compliant with the requirements to ensure the airborne campaign observation performance.

Finally, the thermal tests confirm the operational stability of the complete camera system. The CH4 NanoCarb camera operates between 10°C and 29°C, while the CO2 NanoCarb camera operates between 9°C and 30°C. Both results demonstrate an enhanced operational range relative to initial tests.

Overall, the NanoCarb-P camera system satisfies its key optical and thermal specifications and is qualified for airborne operations.